LA-5926-MS
Informal Report

UC-45
Reporting Date: March 1975
Issued: June 1975

24 3

Time-Dependent Detonations

J. B. Bdzil
W. C. Davis

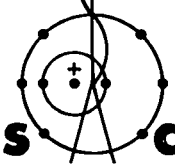

los alamos
scientific laboratory
of the University of California
LOS ALAMOS, NEW MEXICO 87544

UNITED STATES
ENERGY RESEARCH AND DEVELOPMENT ADMINISTRATION
CONTRACT W-7405-ENG. 36

In the interest of prompt distribution, this report was not edited by the Technical Information staff.

Printed in the United States of America. Available from
National Technical Information Service
U S Department of Commerce
5285 Port Royal Road
Springfield, VA 22151
Price: Printed Copy $4.00 Microfiche $2.25

TIME-DEPENDENT DETONATIONS

by

J. B. Bdzil and W. C. Davis

ABSTRACT

We describe a one-dimensional time-dependent model for high-order detonations. In the model most of the available energy is released instantaneously, while a small fraction $\delta^2 \simeq 0.05$ is released on a slow time scale $1/k_2 \simeq 0.5$ μs. An analytic solution of the model in the polytropic gas and Euler approximations is found as a perturbation series in δ. This solution shows that the apparent Chapman-Jouguet pressure increases by $O(\delta)$ on a time scale $\delta k_2 t$, while the actual Chapman-Jouguet pressure and detonation velocity increase by $O(\delta^2)$. Calibrated to the Composition B/dural free-surface velocity experiments, the model reproduces all of the known planewave experiments on Composition B. The model is also calibrated to the PBX-9404/dural data. Although it reproduces the free-surface velocity data, it does not agree with all the data on this explosive. The solution of this model represents the first analytic solution of the time-dependent detonation problem.

I. INTRODUCTION

The Chapman-Jouguet theory of unsupported detonations has met with reasonable success in describing explosions. This has in large measure been due to an inability to perform either experiments or calculations with sufficient accuracy to test the assumptions of the theory. This theory makes the following assumptions: (1) The flow is plane and one-dimensional; (2) the reaction occurs instantaneously producing discontinuous jumps in the flow variables; (3) the flow at this shocked state (the Chapman-Jouguet state) is exactly sonic relative to the velocity of the discontinuity; and (4) the following flow is isentropic. During the past 15 years, however, more sensitive experiments have shown that one or more of these assumptions are violated. Working with the gaseous explosive hydrogen/oxygen, White[1] showed that the flow behind the shock was three-dimensional. The time scale for the decay of these motions was shown to be large with the flow at the end of the decay being supersonic. Thus, for this explosive, at least two of the assumptions of the Chapman-Jouguet theory are violated. For solid and liquid explosives the situation is much the same. Davis, Craig, and Ramsay[2] have shown that the Chapman-Jouguet theory fails to work for nitromethane and TNT. Following a procedure described by Wood and Fickett[3] they found that the sonic-plane pressures for these explosives were 10 to 15% below the Chapman-Jouguet pressure measured by the free-surface technique proposed by Goranson.[4] Using free-surface velocity measurements, Craig[5] found that the Chapman-Jouguet pressure increases with the length of explosive for planewave assemblies of the solid explosive PBX-9404. In addition, his data failed to scale, which is contrary to the Chapman-Jouguet theory. We find similar departures from the simple theory for Composition B. Another indication that the simple theory has failed is that there seems to be little agreement on what the value of the Chapman-Jouguet pressure is for an explosive.

The quoted values for Composition B-3 range from 26.8 to 31.2 GPa.[6]

More recently it has become possible to do very accurate calculations on one-dimensional explosive systems using finite-difference methods and high-speed computers. These calculations show that if the simple theory is used to describe the explosive, then the free-surface velocity induced into inert materials by large explosive charges cannot be reproduced even with the most sophisticated equations of state for the inert.[7] The calculated slope of the free-surface velocity induced in aluminum by a charge of Composition B 203-mm long and 254 mm in diameter is about half as steep as Deal's[8] measured value. Thus, both experiment and calculation show that the behavior of solid and liquid explosives is also considerably more complex than that allowed by the Chapman-Jouguet theory.

What we will do in this report is turn the contradictions of the experiments and theory to our advantage. In particular, we assume that the experimental results and calculations are meaningful and that the differences between them and the Chapman-Jouguet theory must be reconciled by any new theory. We will limit the scope of our investigation to only two planewave explosive systems. Composition B will be examined first because of the great wealth of data available on it, followed by PBX-9404. The conflict between data and theory for these explosives suggests that any new model must have the following features. (1) The near constancy of the detonation velocity as measured with rate sticks requires that the greater part of the energy in a detonation is released instantaneously in the shock rise just as in the Chapman-Jouguet theory. (2) Both the increase in the initial free-surface velocity with length of explosive and the steepness of the free-surface velocity curve for large charges implies the existence of a weakly-energetic, slow kinetic process following the initial energy release. (3) This in turn implies that the detonation is time-dependent. (4) The initial state variation experiments on other explosives suggest that the pressure at the sonic plane is considerably lower than those measured by free-surface velocity techniques. All of these features can be included in a model by adding two parameters to the existing theory--one, to give the amount of energy released in the slow kinetic process, and the second,

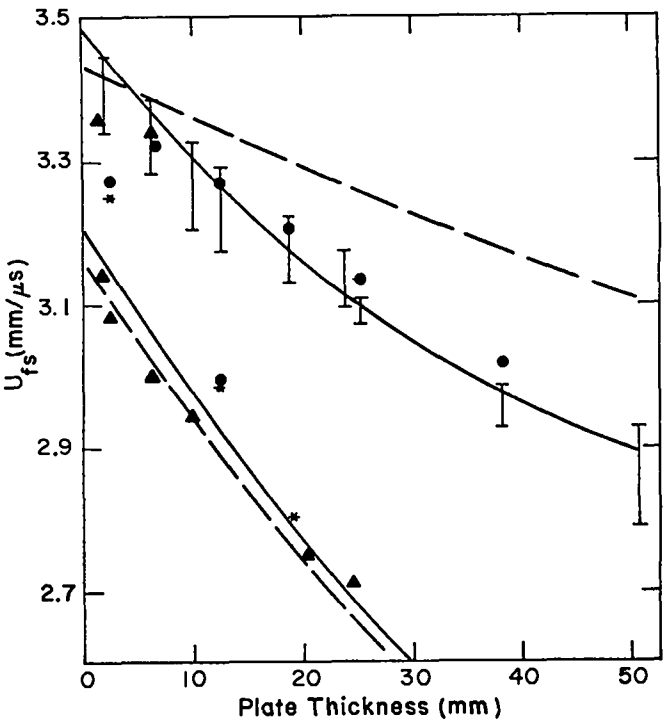

Fig. 1.1. A comparison of the free-surface velocity induced in dural plates by a 50.8-mm (lower) and 203.2-mm (upper) planewave Composition B system. The solid curve is the new theory and the dashed curve is the Chapman-Jouguet theory (γ-law calibrated to produce the correct intercept). The data shown are those of W. E. Deal,[8] who used an armored flash gap technique, and W. C. Davis,[6] who used a reflection-change flash gap technique. Davis' data are reduced by 6% to correct for the effects of surface fluff. The length to diameter ratios of the explosives (X/d) are

Deal X/d=1 ●, I X/d=½ ✱

Davis X/d=¼, ½, 1 ▲

the rate of the process. By calibrating these and the remaining constants to the available experimental data, one can then reproduce all of the planewave experiments on Composition B with one set of parameters. An example of what can be achieved with the new theory as compared to the old is shown in Fig. 1.1. The agreement between calculation and experiment is good. This improvement over existing theories is achieved because we have abandoned the notion that discrepancies between calculation and experiment can be removed by using an "improved" equation of state. The experimental data clearly

show that the system Composition B/dural does not scale. Therefore, any calculation which scales is doomed from the start. To our knowledge, the only other work which takes into account some aspects of the failure to scale are calculations performed by Mader.[9,10]

The body of this report is divided into six sections. In Section II we discuss the experiments which are commonly used to characterize high explosives. We then present the experimental data on planewave Composition B and discuss the inability of simple theories to describe the data. In Section III we present our time-dependent two-reaction model and obtain a solution to the governing equations. We discuss the solution of the finite-difference equations for our model and the accuracy of such a solution in Section IV. In Section V we calibrate the model to Composition B and compare the results of calculation and experiment. In Section VI we calibrate the model to PBX-9404 and compare calculation and experiment. We summarize our results in the last section and discuss some of the implications of the model, and speculate on directions for future work.

II. EXPERIMENT AND THE CHAPMAN-JOUGUET THEORY

A. Survey of Experimental Methods

Quite early in the study of detonations researchers learned that the detonation velocity could be measured reproducibly. Their experiments showed that to within 1 or 2% the detonation velocity in gases was constant and in good agreement with the predictions of the Chapman-Jouguet theory. Because of this the theory gained wide acceptance. Unfortunately, the detonation velocity is probably one of the least sensitive parameters characterizing an explosive. For this reason, very little was learned about explosives until both the experimental techniques and theory were improved during the 1940s. The Chapman-Jouguet theory was modified independently by Zeldovich, von Neumann, and Doering (ZND) to include a steady-state chemical reaction zone in which the pressure decreases between the shock discontinuity and the Chapman-Jouguet state. They reasoned that the reaction zone was short and, therefore, the assumption of steadiness was justified. On the experimental side the emphasis had shifted to solid explosives. Goranson[4] suggested that for solid explosives the reaction zone could be probed and its existence established by measuring the initial free-surface velocity imparted to metal plates as a function of plate thickness. This technique is based on the fact that the shock and following pressure profile in the explosive are transmitted into the inert. In the inert the flow following the shock is subsonic and therefore degrades the shock as it runs. Since plate thickness is directly related to run in the inert, we can sample different parts of the detonation profile by varying the plate thickness. If an equation of state for the inert is available the data can be deconvoluted (at least approximately) to get the wave profile in the explosive and the Chapman-Jouguet pressure.

The first published work in which this technique was used to study an explosive was that of Duff and Houston[11] (1955) on Composition B. They interpreted their results as showing the existence of the reaction zone spike predicted by the ZND theory. A few years later Deal[8,12] (1957, 1958) published the results of an exhaustive series of free-surface velocity experiments on 203.2-mm long planewave systems of Composition B, RDX, TNT, and Cyclotol initiated by planewave lenses of 203-mm aperture. His work on Composition B, which included a number of different materials as witness plates, constitutes the largest single source of data on this explosive. In addition to this work, Deal also studied some shorter planewave systems.[13] All of these measurements were made using a rotating-mirror smear camera to time the free run of the witness plate over a predetermined distance. This distance (2.5 mm) was chosen so as to exclude the possibility of any reverberations of the witness plate. The arrival times were measured using armored (steel) flash gaps (0.089 mm) at both ends of the free run distance. Some 10 years later, Davis[14] also performed free-surface velocity measurements on Composition B. The free run time in these experiments was determined by first optically measuring the time that the reflectivity of the witness plate changed and then the time at which a luminous shock was generated when the flying plate collided with a Plexiglas flasher at the end of the run. This technique has the advantage of allowing one to resolve any differences in plate motion that may occur over the surface of the plate, thereby providing some measure of the one-dimensionality of

the system being studied. Using an electrical pin technique, Warnes[15] also measured the free-surface velocity in an independent set of experiments. The experiments described here are just a few of the free-surface velocity measurements that have been made on Composition B. However, we will restrict our attention to the aforementioned experiments because we lack specific details of the experimental conditions under which the remaining work was performed.

Other techniques have also been used to calibrate liquid and solid explosives. The shock-velocity technique developed by Hayes[16] (1967) has enjoyed widespread use. This technique is based on the experimental observation that a shock crossing a material interface produces a characteristic electrical signal which is detectable with suitably arranged antenna and amplifier systems. Such a signal is produced when two pieces of the same material are separated by a vanishingly thin insulating layer. Therefore, if a stack of such sandwiches is placed on top of a planewave explosive charge, the transit times of the induced shock over the known distances between the insulating layers can be measured. If the equation of state of the inert is known, these transit times can be used to infer the Chapman-Jouguet pressure in the explosive. This method has the advantage of yielding more than one measurement per experiment. Recently, Finger and Kurrle[17] used this method to measure the Chapman-Jouguet pressure of Composition B, PBX-9404, plus a number of other common solid explosives.

Both of the methods described above are indirect methods in that one must infer the behavior of the explosive by measuring features of the pressure wave induced into inerts by the explosive. Direct methods for studying explosives are also available. Of these flash radiography is probably used the most frequently.[18] A high-flux x-ray machine, such as PHERMEX, provides one with a snapshot of the density distribution in the explosive products at any time. Two experiments which have been performed using flash radiography are of particular interest. In the first experiment a number of very thin (12.5 μm) high-contrast metal (Ta) foils are embedded in between pieces of explosive creating a multi-layered sandwich. These foils are all parallel to the detonation front and their initial positions are known precisely. Assuming that the foils have a negligible effect on the flow, acting merely as fluid particle labels, then a radiograph of the assembly taken after the detonation has run some distance yields the density distribution at that time. If then a series of such experiments is performed, with radiographs taken after different lengths of run, the flow field in the explosive gases can be determined without any assumptions about the equation of state. Using this technique, Rivard et al.[19] determined the following flow in a 101.6-mm planewave system of Composition B. The second experiment uses flash radiography to follow the rarefaction head reflected into the explosive gases when a plane detonation wave interacts with a low impedance inert. The advantage of this experiment is that is does not require the use of foils; and, therefore, the foil perturbations are eliminated. From a series of such experiments, the position of the rarefaction head in the explosive products can be determined as a function of time and in turn these data can be deconvoluted to give the flow in the explosive. Davis and, Venable[6] have published the results of such a series of experiments on Composition B.

Another technique which gives a direct measure of the flow behind the detonation front is the magnetic probe technique introduced by Hayes.[20] By embedding a highly conductive metal foil in the explosive, the velocity of the foil, which serves as a particle marker, can be measured directly. Unfortunately the data on Composition B obtained with this method are too limited to be useful.

Before discussing the experimental data we present a brief summary of the methods and give some indications of their sensitivity. The methods are of two basic types: (1) the indirect type in which the experimenter infers properties of the explosive by observing the inert in an explosive inert system; (2) the direct type in which the experimenter probes the explosive directly. In each of these categories the sensitivity of the experiments varies. Those providing the particle velocity u directly give a more sensitive description of the flow following the detonation front than those which give only an integral of u (see Fig. 2.1). The shock velocity experiments determine the upper limit of the integral

Indirect

A. Free-surface velocity vs plate thickness
   Determine u

B. Shock velocity using stacked plates and electrical pick up
   Determine D_I

Direct

A. X-ray technique
   Determine $X_F = X_I + \int u dt$ of embedded foils

B. X-ray technique
   Determine rarefaction wave velocity

C. Magnetic probe

Fig. 2.1. Experimental methods used in studying solid explosives.

$$\Delta X_S = \int_{t_1}^{t_2} D_I(u)dt \quad , \tag{2.1}$$

where ΔX_S is the distance traveled by the shock in the inert and D_I is its velocity. The embedded foil experiments give

$$X_F = X_I + \int u dt \quad , \tag{2.2}$$

where X_I and X_F are the initial and final foil positions, respectively, and u is the particle velocity in the explosive. Similarly the rarefaction head experiments give

$$X_R = X - \int (c-u)_R dt \quad , \tag{2.3}$$

where X_R is the position of the rarefaction head, X is the length of the explosive, and c is the local speed of sound. Therefore, data from free-surface velocity and magnetic probe experiments provide us with the most detailed view of the profile following the detonation wave. Since we have no data obtained using the magnetic probe, our work will rely heavily on the free-surface velocity measurements. This is unfortunate for two reasons. First, the data on free-surface velocities only probe back 10 mm into the explosive gases. Second, we cannot be certain that we fully understand how to interpret the data.

B. Free-Surface Velocities

The free-surface velocity measurements on Composition B were made over a period of 14 years.

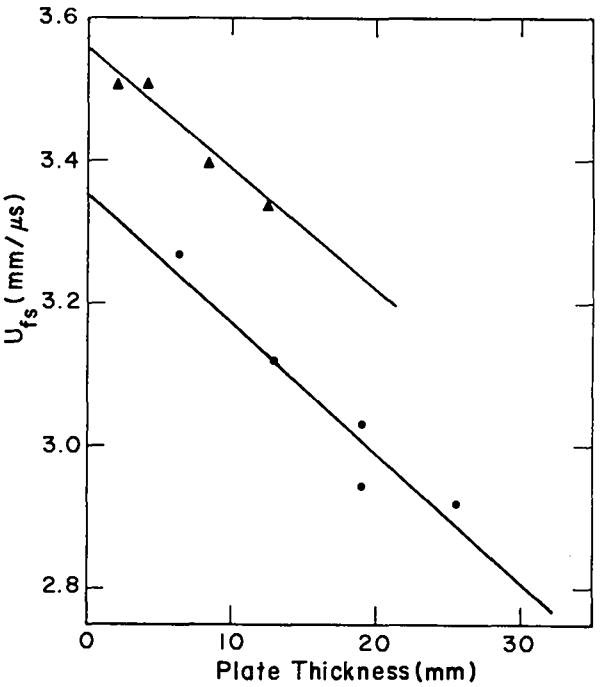

Fig. 2.2. A plot of the free-surface velocity vs thickness for a 101.6-mm-long x 101.6-mm diam (X/d=1) planewave Composition B/dural system. The explosive was initiated by a planewave lens of 203.2-mm aperture.

Deal ● Davis ▲

During that time the formulation changed from 64% RDX/36% TNT (by weight) ρ_o = 1.71 Mg/m^3 at the time of Deal's[8] measurements, to 60% RDX/40% TNT, ρ_o = 1.73 Mg/m^3 at the time of Davis'[14] measurements. To first order the changes in the energy and density are just compensating and we will not make any distinctions between these two formulations. The techniques used by Deal and Davis to measure the free-surface velocity are sufficently different to warrant some comment. Both techniques employ a rotating-mirror smear camera to time the flight of the free surface over a fixed free-run distance. Deal's technique is symmetric in that he used armored argon flash gaps (0.089 mm) at both ends of the run. On the other hand, Davis equated the change in reflectivity of the free surface with the start of the free run and the appearance of a luminous air shock

generated by the arrival of the plate at a plastic flasher with the end of the run. Figure 2.2 shows that the two techniques produce different results for a 101.6-mm-long x 101.6-mm-diam (X/d = 1) plane-wave Composition B/dural system. Although Davis' data have the same slope as Deal's, his values are consistently higher by about 6%. This difference is probably attributable to the greater sensitivity of Davis' technique to surface fluff. However, it would be difficult to judge which technique is the more accurate. In lieu of such a judgement, we will reduce Davis' data by 6% to bring them into agreement with Deal's. We choose this alternative because Deal's method is used in calibrating the equation of state of inerts which we will require in our calculations, and because he collected more data over a wider range of materials and plate thicknesses.

Before we proceed with an analysis of the data, we must determine which if any data sets belong to the family of plane one-dimensional experiments. The precise definition of a one-dimensional system is relaxed somewhat in this report to include the three-dimensional structure of the planewave driver and the reaction zone, but still reject any gross multi-dimensionality resulting from side rarefactions. We can get some measure of the effect that side rarefactions have on the data by comparing free-surface velocity data for charges of the same length but of different diameters. Figures 2.3a and 2.3b show the free-surface velocity for a number of different length-to-diameter ratios (X/d) for both 101.6-mm and 203.2-mm-long charges. The data for the 101.6-mm-long experiments show that the data taken for systems with X/d=½ and X/d=1 belong to the same set, while the two data points for X/d=2 are significantly lower. Examining the data for the 203.2-mm-long experiments shows that the data for X/d=1 and X/d=2 are clearly distinguishable. Thus, these data suggest that systems with a length-to-diameter ratio of

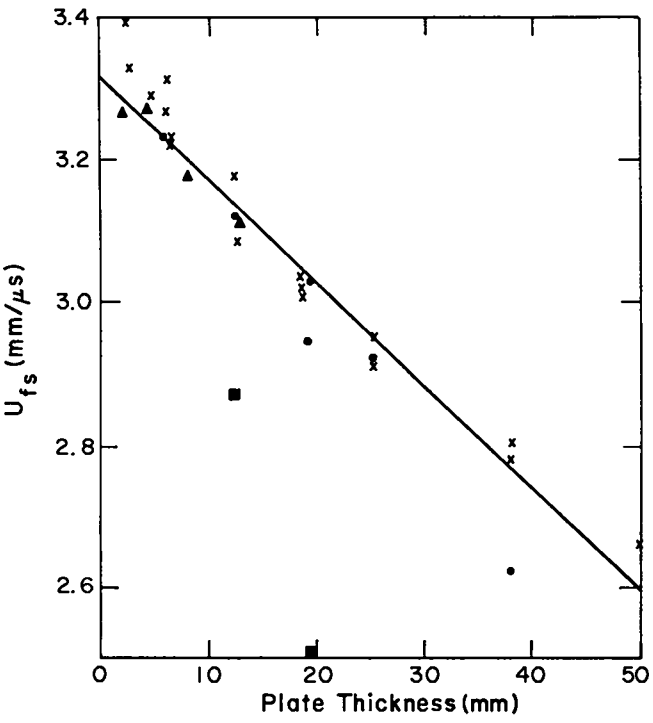

Fig. 2.3a. A plot of the free-surface velocity vs thickness for some 101.6-mm-long plane-wave Composition B/dural systems showing the dependence on X/d.

Deal X/d=½ X X/d=1 ● X/d=2 ■

Davis/1.06 X/d=1 ▲

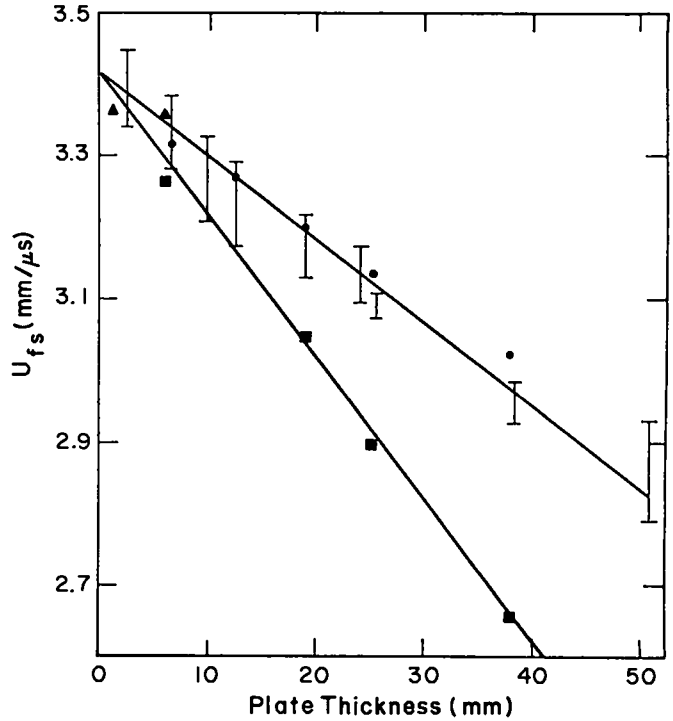

Fig. 2.3b. A plot of the free-surface velocity vs thickness for some 203.2-mm long plane-wave Composition B/dural systems showing the dependence on X/d.

Deal X/d=1 I X/d=1 ● X/d=2 ■

Davis/1.06 X/d=1 ▲

the explosive less than or equal to one and dural plate thickness up to about 40 or 50 mm can properly be classed as one-dimensional. The technique used by Davis is especially well suited to judge the dimensionality of the experiment since it gives the local values of the free-surface velocity over the surface of the witness plate. Figure 2.4 shows that the free-surface velocity is reasonably constant over the central region of the plate and falls rapidly in the region that has been influenced by side rarefactions. By extrapolating the length of this plateau to zero plate thickness we get the dimension of the region of one-dimensional flow in the explosive. Experiments on Composition B show that the ratio of the velocity of the side rarefaction in the explosive to the detonation velocity is about 1/4.[21] That is, the outer 13 mm of a 50.8-mm-long charge and the outer 50 mm of a 203.2-mm-long charge induce free-surface motions into dural that show the effects of side rarefactions for all plate thicknesses. The effect that side rarefactions have on the flow in the inert is greater owing to the absence of an exothermic process there. This difference leads to a flow in the inert which is strongly subsonic for some distance behind the shock as compared to the flow in the explosive which is sonic at the shock and supersonic thereafter. Figure 2.4 shows the results of a series of experiments on 50.8-mm-long x

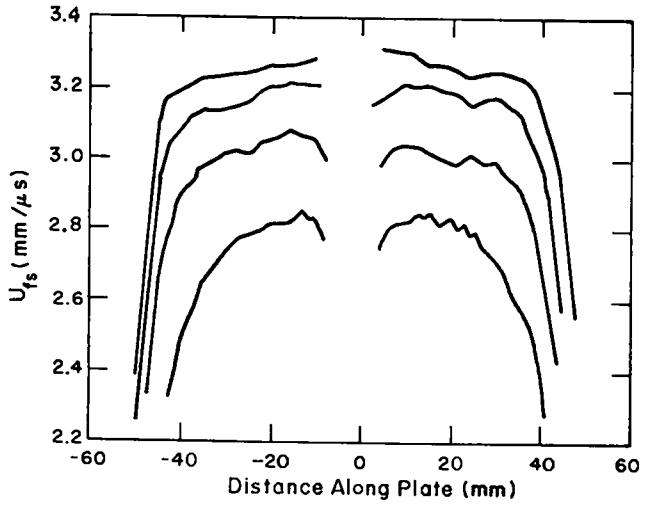

Fig. 2.4. The free-surface velocity vs distance along the plate for a charge of Composition B 50.8-mm long x 101.6-mm diam driving 1100F Al.[22] The plate thicknesses are 2.54 mm, 5.08 mm, 10.16 mm, and 20.32 mm.

TABLE II-1

THE LIMITS OF ONE DIMENSIONALTY FOR PLANEWAVE COMPOSITION B/Al

Composition B Length (mm)	X/d	Maximum Al Thickness (mm)
50.8	1/2	40
	1	15
101.6	1/2	75
	1	25
203.2	1	50

101.6-mm-diam charges of Composition B driving 1100F Al plates of 4 different thicknesses. These experiments show that the ratio of the velocity of the side rarefaction to the velocity of the shock is about equal to the theoretical maximum of one. Therefore, the region of one-dimensional flow in the Al is bounded by a right equilateral triangle whose base rests on the Composition B/Al interface. Applying these results we obtain an estimate of the maximum Al plate thickness that can be used with various lengths of explosive (see Table II-1). Using the criteria established here we must reject Deal's 38-mm dural point for X/d=1 and 101.6 mm of explosive. Examination of Fig. 2.3a confirms this conclusion. Therefore, in light of the experimental evidence, the greater part of the free-surface velocity data on Composition B/dural must be considered as one-dimensional. The number of experiments which have been directed to the question of multi-dimensional flow in these systems is not large and perhaps all of the interesting questions have not been answered. Nevertheless we feel that our conclusion is substantially correct.

All of the one-dimensional free-surface velocity data on 24.5-mm, 50.8-mm, 101.6-mm, and 203.2-mm-long charges of Composition B/dural are shown in Fig. 2.5. A linear fit to each of the data sets suggests that the initial free-surface velocity increases with the length of the charge. Although the scatter in the data is large, the intercept for the 25.4-mm and 203.2-mm-long charges differ by 0.3 mm/μs, which is well outside of experimental error. If we interpret this increase in the initial free-surface velocity $U_{fs}|_o$ as showing an increase in pressure in the explosive, then the flow of explosive gases does not scale, which is in violation of the Chapman-Jouguet theory.

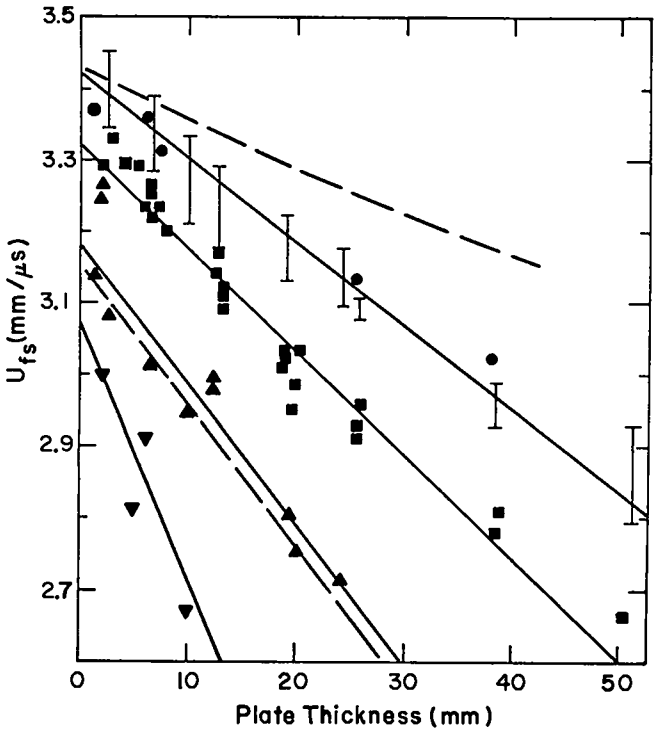

Fig. 2.5. Free-surface velocity vs plate thickness data (Deal, Davis) for a one-dimensional Composition B/dural system. The charge lengths are 203.2 mm (●), 101.6 mm (■), 50.8 mm (▲), and 25.4 mm (▼). The dashed lines are the result of calculations made using γ-law equations of state for the explosive gases and a Mie-Grüneisen equation of state (LA-4167-MS) for the dural data. (See Fig. 1.1)

Most of the free-surface velocity measurements that have been made on explosive-driven inerts were motivated by a desire to measure the Chapman-Jouguet pressure of the driving explosive. The explosive pressure is calculated by extrapolating the free-surface velocities to zero plate thickness and then performing an impedance match into the explosive gases with this value. A check on the self-consistency of this procedure can be made by taking the pressure so measured and a reasonable equation of state for the gases and then computing the free-surface velocity curve. Such a series of calculations was done using a γ-law equation of state for the explosive gases with γ selected so as to reproduce the measured value of $U_{fs|o}$. The results of these calculations (the dashed lines) are shown in Fig. 2.5. The agreement between calculation and experiment is good for the 50.8-mm-long charge. However, one finds that the calculation and experiment are in gross disagreement for the 203.2-mm-long charge. One possible explanation for the poor agreement is that our description of the inert (Mie-Grüneisen fluid) is not adequate. Modifying our calculation to include an elastic perfectly plastic description of dural[23] steepens the free-surface velocity curves. Unfortunately, the increase is small and the slopes are increased by the same percentage for both charge lengths.

Since all of the above calculations are based on the assumption that the explosive gases can adequately be described by a constant γ equation of state, it is worthwhile to ask whether any other equation of state for the explosive gases will produce better agreement between the calculated and experimental slopes for long charges. If one assumes that the curvature of the free-surface velocity curves is not large, he can answer this question with a simple analytical calculation. The success of this calculation hinges on one's knowing the gradient in the following flow at the Chapman-Jouguet point for any equation of state at any time. Our starting point is the one-dimensional Euler equations

$$\left(\frac{\partial v}{\partial t}\right)_h - \frac{1}{\rho_o}\left(\frac{\partial u}{\partial h}\right)_t = 0 \quad , \tag{2.4}$$

$$\left(\frac{\partial u}{\partial t}\right)_h + \frac{1}{\rho_o}\left(\frac{\partial P}{\partial h}\right)_t = 0 \quad , \tag{2.5}$$

$$\left(\frac{\partial E}{\partial t}\right)_h + P\left(\frac{\partial v}{\partial t}\right)_h = 0 \quad , \tag{2.6}$$

where v is the specific volume of our fluid, ρ_o the initial density, u the particle velocity, P the pressure, E the internal energy, t the time, and h the material coordinate. The Eulerian space variable $\zeta = \zeta(h,t)$ is related to the Lagrangian variable by

$$\left(\frac{\partial \zeta}{\partial h}\right)_t = \frac{\rho_o}{\rho} \quad , \tag{2.7}$$

$$\left(\frac{\partial \zeta}{\partial t}\right)_h = u \quad . \tag{2.8}$$

If we assume that the flow is non reactive then Eq. (2.6) can be rewritten as

$$\left(\frac{\partial P}{\partial t}\right)_h + z^2\left(\frac{\partial v}{\partial t}\right)_h = 0 \ , \qquad (2.9)$$

where $z = \rho c$ is the impedance of the fluid. Since we are assuming a Chapman-Jouguet detonation, the detonation wave is a singular surface across which u, P, v, and E suffer jump discontinuities. The wave velocity as seen by an observer fixed to a material point is

$$U(t) = \frac{d\tilde{h}}{dt} \ , \qquad (2.10)$$

where $\tilde{h}$ is the material point, labeled by its position in the reference configuration, at which the wave is to be found at time t. An observer at rest sees the wave velocity

$$D(t) = \frac{d\zeta(\tilde{h}, t)}{dt} \ . \qquad (2.11)$$

Following Truesdell we denote the jump in a variable across the singular surface by

$$[\psi] \equiv \psi\left(\tilde{h}^-(t),\ t\right) - \psi\left(\tilde{h}^+(t),\ t\right) \ , \qquad (2.12)$$

where the superscripts + and - refer to states ahead of and behind the surface, respectively.[24,25] If $\frac{\partial \psi(h,t)}{\partial h}$ and $\frac{\partial \psi(h,t)}{\partial t}$ are everywhere continuous in h except at the singular surface where they suffer jump discontinuities, then

$$\frac{d[\psi]}{dt} = \left[\frac{\partial \psi}{\partial t}\right] + U\left[\frac{\partial \psi}{\partial h}\right] \ , \qquad (2.13)$$

where $\frac{d[\psi]}{dt}$ is the rate of change of $[\psi]$ seen by an observer riding on the wave front. When $[\psi] = 0$ we get the Maxwell compatibility relation[24]

$$\left[\frac{\partial \psi}{\partial t}\right] = -U\left[\frac{\partial \psi}{\partial h}\right] \ . \qquad (2.14)$$

Since the Eulerian position coordinate is continuous at the wave front, Eq. (2.14) yields

$$[u] = -U\rho_o[v] \ , \qquad (2.15)$$

which expresses the conservation of mass. The balance of momentum implies that

$$[P] = \rho_o U\,[u] \ . \qquad (2.16)$$

Making use of the formalism presented above, it is a relatively simple matter to derive equations which describe the evolution of [P], $\left[\frac{\partial u}{\partial h}\right]$, etc. If we assume that all derivatives are zero in the unshocked state, then application of the jump conditions to Eqs. (2.9), (2.5), and (2.4), along with Eq. (2.13), yields

$$\frac{d[P]}{dt} + \rho_o U \frac{d[u]}{dt} = \frac{1}{\rho_o}\left(\rho_o^2 U^2 - z^2\right)\left[\frac{\partial u}{\partial h}\right] \ . \qquad (2.17)$$

If a constitutive relation is available for the fluid, then the total differentials of [P] and [u] on the Hugoniot curve are related by

$$d[u] = \left(\frac{du}{dP}\right)_H d[P] \ , \qquad (2.18)$$

and Eq. (2.17) can be used to give the evolution of [P] provided $\left[\frac{\partial u}{\partial h}\right]$ is known. To derive an equation for $B \equiv \left[\frac{\partial u}{\partial h}\right]$ we begin with

$$A = \frac{1}{U}\left(\frac{d[P]}{dt} - \left[\frac{\partial P}{\partial t}\right]\right) \ , \qquad (2.19)$$

where $A \equiv \left[\frac{\partial P}{\partial h}\right]$, which, after differentiation, becomes

$$U\frac{dA}{dt} + A\frac{dU}{dt} = \frac{d^2[P]}{dt^2} - \left[\frac{\partial^2 P}{\partial t^2}\right] - U\left[\frac{\partial^2 P}{\partial t \partial h}\right] \ . \qquad (2.20)$$

Applying the jump conditions to Eq. (2.5), taking the total time derivative of the result and then adding the derived equation to Eq. (2.20) yields

$$2U\frac{dA}{dt} + A\frac{dU}{dt} = \frac{d^2[P]}{dt^2} - \left[\frac{\partial^2 P}{\partial t^2}\right] - \rho_o^2 U^2\left[\frac{\partial^2 v}{\partial t^2}\right] \ . \qquad (2.21)$$

Now, taking the partial derivative of Eq. (2.9) with respect to time and then applying the jump conditions gives

$$\left[\frac{\partial^2 P}{\partial t^2}\right] = -z^2\left[\frac{\partial^2 v}{\partial t^2}\right] - \frac{1}{\rho_o^2}\left(\frac{\partial z^2}{\partial v}\right)_S B^2 \ , \qquad (2.22)$$

where $\left(\frac{\partial z}{\partial v}\right)_S$ is the change of impedance with volume at constant entropy. Substituting Eq. (2.22) into (2.21) gives the desired result

$$2U\frac{dA}{dt} + A\frac{dU}{dt} = \frac{d^2[P]}{dt^2} + \left(z^2 - \rho_o^2 U^2\right)\left[\frac{\partial^2 v}{\partial t^2}\right] + \frac{1}{\rho_o^2}\left(\frac{\partial z^2}{\partial v}\right)_S B^2 \quad , \tag{2.23}$$

where we have used the identity

$$B = \frac{1}{U}\left(\frac{A}{\rho_o} + \frac{d[u]}{dt}\right) \quad . \tag{2.24}$$

This excursion into the formalism of singular surfaces was motivated by our need to know the gradient of the particle velocity immediately behind the classical Chapman-Jouguet state. Now, [P] and [u] are constant at the Chapman-Jouguet state. Therefore, it follows from Eq. (2.17) that the flow is sonic and from Eq. (2.16) that U is constant. With these restrictions Eq. (2.23) becomes

$$\frac{dB}{dt} = \frac{\left(\frac{\partial z^2}{\partial v}\right)_S}{2\rho_o z^2} B^2 \tag{2.25}$$

which integrates to

$$B = -\frac{2\rho_o z^2}{\left(\frac{\partial z^2}{\partial v}\right)_S}\frac{1}{t} \quad , \tag{2.26}$$

$$\left(\frac{\partial u}{\partial \zeta}\right)_{CJ} = \frac{2}{\left[1 + \gamma - \left(\frac{\partial \ell n \gamma}{\partial \ell n v}\right)_S\right]}\frac{1}{t} \quad , \tag{2.27}$$

where $\gamma \equiv z^2 \frac{v}{p}$. To get the initial value of the particle velocity gradient in the dural we need perform only a simple acoustic impedance match.

$$\frac{\partial u_2}{\partial \zeta} = 2\left(\frac{z_{12}}{1 + z_{12}}\right)\left(\frac{D_1 - u_c}{u_c + c_2 - u_c}\right)\frac{\partial u_1}{\partial \zeta} \quad , \tag{2.28}$$

where $z_{12} \equiv z_1/z_2$, c is the sound speed, the subscript c denotes the value at the interface after the match, and 1 and 2 refer, respectively, to the explosive before and the inert after the match. The slope of the free-surface velocity is then given by

$$\frac{\partial U_{fs}}{\partial x} = 2\left(\frac{u_c + c_2}{D_2} - 1\right)\frac{\partial u_2}{\partial \zeta} \quad , \tag{2.29}$$

where D_2 is wave velocity in the inert. Specializing this result to 203 mm of Composition B (γ = 2.72, ρ_o = 1.73 Mg/m^3, D_1 = 7.9 mm/μs) and dural (Walsh: LA-4167-MS) gives

$$\frac{\partial U_{fs}}{\partial x} = 0.25\frac{\partial u_1}{\partial \zeta} = 0.5\frac{D_1}{\left[1 + \gamma - \left(\frac{\partial \ell n \gamma}{\partial \ell n v}\right)_S\right]}\frac{1}{X} \quad , \tag{2.30}$$

where X is the length of the explosive. For a constant γ equation of state, Eq. (2.30) gives 0.0053 μs^{-1} as compared to the result obtained by a numerical integration of the difference equations for this system[7] of 0.0052 μs^{-1}. This is only half as steep as Deal's experimental value of 0.0108 μs^{-1}. In order for the calculation to agree with Deal's experimental slope we must have

$$\left(\frac{\partial \ell n \gamma}{\partial \ell n v}\right)_S = 1.89 \quad . \tag{2.31}$$

The value of this derivative calculated from the BKW-HOM and JWL isentropes is -0.23 and 0.76, respectively. Although the JWL isentrope is better than the BKW-HOM at producing a slope of the desired steepness, neither of these calibrated isentropes agrees with the data. It is possible to adjust the parameters in an equation of state so that Eq. (2.31) is satisfied. The simplest example for which this is possible is the Tait equation of state,

$$\frac{P + a}{P_o + a} = \left(\frac{v}{v_o}\right)^{-n} \quad , \tag{2.32}$$

where a and n are adjustable parameters. Adjusting these parameters to get both the proper intercept and slope we get n = 0.83 and a = 66.1 GPa. If this calibration of the Tait isentrope for 203 mm of Composition B is used to calibrate the match pressure into hexane, we get

$$\left(P_{hexane}\right)_{Tait} = 12.5 \text{ GPa} \tag{2.33}$$

as compared to the experimental value[12] of

$$\left(P_{\text{hexane}}\right)_{\text{Deal}} = 14.9 \text{ GPa} \quad . \tag{2.34}$$

Therefore, a calibration of the Tait isentrope to the Composition B/dural U_{fs} intercept and slope fails badly at reproducing the match pressure in another inert. All of this suggests that the observed slope of U_{fs} in a 203-mm-long Composition B/dural planewave experiment can probably not be reproduced by equation of state modifications. Also, Eq. (2.31) requires that γ be a strongly decreasing function of density at the Chapman-Jouguet point, a result which is counter to one's intuition.

Reviewing our work to this point, we find that the U_{fs} measurements on Composition B/dural show an increase in $U_{fs}|_o$ with charge length and that the slope of the U_{fs} curve for large charges is steeper than can be calculated with any reasonable equation of state. If our interpretation of the experimental results is correct, i.e., the inert and explosive/inert interaction are treated properly, then these measurements show that the Chapman-Jouguet theory cannot adequately describe Composition B.

C. Ad Hoc Models

In the preceding section we showed that the simple theory fails to reproduce the measured free-surface velocity for the system Composition B/dural. Here we discuss some ad hoc methods that have been tried to produce improved calculations. We begin by considering a model for reproducing the dural U_{fs} slope for long charges. Introducing a resolved steady-state reaction zone ahead of the sonic plane provides us two additional parameters which can be adjusted to give both the loading pressure and slope of the detonation wave. Modifying Eq. (2.17) so as to include the effects of reactions, the gradient of the particle velocity at any point in the steady reaction zone is given by

$$\frac{\partial u}{\partial \zeta} = \frac{\rho}{E_P} \frac{\underline{q}\cdot\underline{r}}{\left(\rho_o u^2 - z^2\right)} \quad , \tag{2.35}$$

where $\underline{q}$ and $\underline{r}$ are the energy and reaction rate vectors, respectively, and $E_P \equiv \left(\frac{\partial E}{\partial P}\right)_v$. Specializing this equation to a single irreversible exothermic reaction and a γ-law equation of state, we get

$$\frac{\partial u}{\partial \zeta} = \frac{q_1}{u^2} \frac{(\gamma - 1)\, r_1}{\left(1 - \frac{P}{\rho_o u^2}\right)\left((\gamma+1)\frac{P}{\rho_o u^2} - 1\right)} \quad . \tag{2.36}$$

The initial density and shock velocity of the explosive are considered as given. The rate r_1, at least its average value, is constrained so as to produce the reaction zone length needed to reproduce the U_{fs} curve in dural. For the sake of simplicity, we assume the rate law

$$r_i = k_i \left(1 - \lambda_i\right)^{1/2} \quad , \tag{2.37}$$

where k_i and λ_i are the rate constant and progress variable ($\lambda_i = 0$, no reaction; $\lambda_i = 1$, complete reaction), respectively. We take k_i as constant and equal to 2 μs^{-1}. The pressure at the shock,

$$P = \frac{2\rho_o u^2}{\gamma + 1} \quad , \tag{2.38}$$

is adjusted by selecting γ ($P = 29$ GPa, $\gamma = 6.44$). If the value of the scaled energy release is set to $\frac{q_1}{u^2} = 0.002$ at the shock front, then the observed initial U_{fs} slope for 203-mm Composition B/dural is obtained. Further, assuming that both γ and $\frac{q_1}{u^2}$ are functions of λ_i, a reaction zone profile suitable to produce the entire U_{fs} curve in dural can be generated. To achieve this, γ must be decreased monotonically from 6.4 to 3.0 while $\frac{q_1}{u^2}$ is increased. This change in stiffness of the equation of state produces partial reaction Hugoniots that cross in the P vs u plane. In turn this leads to an unphysical shock match into low impedance materials such as Plexiglas, with the match pressure rising instead of falling as we pass through the reaction zone.

This deficiency can be corrected by expanding our concept of a reaction zone to include two rate processes: a very fast and energetic process followed by a slow, weakly energetic process. The first reaction is tailored so that its reaction zone thickness is vanishingly short and its energy release is equal to that necessary to produce the initial pressure measured by the free-surface velocity technique. The second is tailored to produce a pressure ramp of the desired slope and length. Because of the added

number of degrees of freedom introduced by the second reaction, the heat-release coefficient can be constant and γ can be selected with equation-of-state considerations being of prime importance. Assuming a constant γ equation of state ($\gamma = 3.15$), Eq. (2.37) with $k_2 = 2\ \mu s^{-1}$ as a rate law, a ratio of the heat release in the second reaction to the total of $\frac{q_2}{q_1 + q_2} = 0.018$, and a pressure of 29.4 GPa at the end of the first reaction zone, we can reproduce the initial free-surface velocity of dural plates driven by 203 mm of Composition B. This is achieved without introducing anomalous impedance matches for other inerts. Therefore, it appears that what could not be achieved with purely equation-of-state considerations is attainable if we follow the instantaneous chemical reaction of the Chapman-Jouguet theory by a weakly energetic reactive flow with a long relaxation time. Clearly, if any rate process in our model is slow, the assumption of steadiness cannot be satisfied for any reasonable size explosive charges. Therefore, if these concepts are to be applied to real explosive systems, then we must face up to the problem of time-dependent detonations. The increase in $U_{fs}|_o$ with length of explosive shows that some relatively slow relaxation process must be important to a description of the detonation process. Thus, it would appear that a time-dependent flow, in basic character like that described here, could bring theory and experiment into better agreement.

The phenomenon of increasing $U_{fs}|_o$ with explosive length has been modeled by Mader.[9,10] As in the Chapman-Jouguet theory, he considered that all the chemical energy is released instantaneously across the shock jump with the flow at the shocked state being sonic. To produce a $U_{fs}|_o$ intercept that increases with explosive length, the amount of chemical energy released by the explosive was taken to increase with time. Since the detonation velocity is related to the amount of energy released ahead of the sonic plane, he decreased the γ of the explosive with run so as to agree with the experimental observation of a nearly constant detonation velocity. Using the $U_{fs}|_o$ data generated by Craig[5] for dural plates driven by different lengths of the solid explosive PBX-9404, Mader calibrated γ (his only available parameter) so as to reproduce the observed $U_{fs}|_o$. So calibrated, his model is capable of reproducing the free-surface velocity curves for PBX-9404/dural for charges up to 50 mm in length. For longer charges the calculated and experimental free-surface velocity slopes differ by a factor of two. Since one is reasonably certain that the longer systems are one-dimensional, this result suggests that his model is incomplete.

All of the proposed changes of the Chapman-Jouguet model that have been discussed are based on discrepancies between calculation and experimental measurements of dural free-surface velocities. It is, therefore, of some interest to compare the simple theory with some of the altered versions of the theory at reproducing different types of experiments. Unfortunately, the other experimental results that are available do not provide a test which is as

TABLE II-2

SHOCK TRANSIT TIMES[a]

x/2X	X = 25 mm t(μs)/2	X = 51 mm t(μs)/4	X = 102 mm t(μs)/8
0.025	0.085 ± 0.005[b]	0.085[b]	0.084[b]
0.050	0.171	0.170	0.169
0.075	0.259	0.256	0.254
0.100	0.347	0.344	0.341
0.125	0.439	0.432	0.427

x/2X	X = 51 mm t(μs)/4	X = 102 mm t(μs)/8	X = 102 mm t(μs)/8
0.025	0.085[c]	0.085[d]	0.086[e]
0.050	0.168	0.169	0.173
0.075	0.254	0.253	0.256
0.100	0.341	0.339	0.341
0.125	0.427	0.424	0.428

[a] Transit times for Composition B induced shocks in dural. The length of the plate and explosive are x and X, respectively. The diameter of the explosive is 101 mm. The deviation ±0.005 represents an estimate of the magnitude of the error in the experimental measurement. All calculations were done with dural as an elastic, perfectly plastic fluid (see Fig. 4.6).

[b] Finger and Kurrle[17]

[c] Mader's model ($\rho_o = 1.73\ Mg/m^3$, $D = 7.85$ mm/μs, $\gamma = 2.98$)

[d] Chapman-Jouguet model ($\rho_o = 1.73\ Mg/m^3$, $D = 7.85$ mm/μs, $\gamma = 2.76$)

[e] Steady two-reaction model

sensitive as that provided by the free-surface velocity measurements. Table II-2 shows some transit times for Composition B induced shocks in dural. The experimental values are the result of measurements performed by Finger and Kurrle.[17] The calculated values are those obtained with the Chapman-Jouguet theory, Mader's model, and a steady-state two-reaction model adjusted so as to produce the experimentally observed free-surface velocity curve for a 101-mm-long charge. As is apparent, the transit times do not change significantly in going from model to model and all of the calculated values agree with experiment. What this exercise suggests is that all of the remaining experiments are sufficiently insensitive so as to permit considerable flexibility in modeling the free-surface velocity measurements.

III. A TIME-DEPENDENT TWO-REACTION DETONATION

Our examination of the Composition B/dural free-surface velocity measurements showed that a two-reaction detonation model would produce better agreement between calculation and experiment than was possible with existing theories. The apparent constancy of the detonation velocity and the fair qualitative description of explosions given by the Chapman-Jouguet theory imply that most of the available chemical energy in the explosive is given up very rapidly. For these reasons we assume that the first reaction is both very exothermic and instantaneous as in the simple theory. It is followed by a slow process of arbitrary thermicity. A number of possible mechanisms for the slow process present themselves. Erpenbeck[26] has shown that even the simplest steady-state one-dimensional reaction zone models are not stable to small perturbations. Considering the complexity of real reaction zones, it seems unlikely that the flow will be laminar in any real explosive. This in turn implies that some of the chemical energy of the explosive is used to drive velocity fluctuations that are transverse to the mean flow. If these motions decay relatively slowly, as they do in gaseous explosives, then their decay might well serve as the second rate process.[27] For Composition B another candidate for the slow process is carbon coagulation. The explosive products of Composition B are known to contain a considerable amount of solid carbon. Since the agglomeration of carbon atoms to form particles is probably limited by diffusion, such a process could also be a relatively slow kinetic step. Unfortunately, the available data do not permit us to determine the nature of the second rate process. For the purposes of modeling, however, it is sufficient to know that such a process probably exists.

The detonation model we propose makes the following assumptions: (1) The energy release is a linear function of the n variables λ_i which describe the progress of n parallel reactions ($\lambda_i = 0$, all reactants; $\lambda_i = 1$, all products). (2) The energy q_1 released by the first reaction is most of the total energy; i.e., if $q = \sum_{i=1}^{n} q_i$, then

$$\frac{q - q_1}{q} = O(10^{-2}) \tag{3.1}$$

where

$$q > 0 \quad . \tag{3.2}$$

(3) The first reaction is irreversible and its time scale is sufficiently short compared to the times over which measurements are made on the explosive to allow us to assume it is instantaneous. (4) The other reactions are slow compared to measurement times. (5) The flow is governed by the one-dimensional Euler equations (for a discussion of the mean flow equations for a turbulent fluid see Ref. 27), with Eq. (2.9) replaced by

$$\left(\frac{\partial P}{\partial t}\right)_h + z^2 \left(\frac{\partial v}{\partial t}\right)_h = \frac{1}{E_p}\left(q_1 r_1 + \sum_{i=2}^{n} q_i r_i\right) . \tag{3.3}$$

(6) The region of reactive flow is followed by an isentropic release wave. Equations (3.3),(2.37),(2.5), and (2.4) together with a suitable equation of state for the fluid provide a complete description of the flow in any region of the fluid in which the flow variables and all of their derivatives are continuous. At the detonation front (the only surface of discontinuity we consider), the flow variables must satisfy the three Rankine-Hugoniot conditions. These three boundary conditions, a suitable set of initial conditions, and the governing equations constitute a compatible system if, and only if, the shock front (the front pressure, etc.) follows a prescribed curve in

the [P] vs t plane. For our model to be of any use, this curve, which is implicitly contained in the governing equations and boundary conditions, must be obtained. This can be done by solving the ordinary differential equations which describe the time rate of change of the jump discontinuities across the detonation front.

Following the procedure used in Sec. II B we readily obtain

$$\frac{d[P]}{dt} = \frac{\frac{1}{\rho_o}\left(\rho_o^2 U^2 - z^2\right)\left[\frac{\partial u}{\partial h}\right] + \frac{1}{E_p}\left[\sum_{i=2}^{n} q_i r_i\right]}{\left(1 + \rho_o U\left(\frac{du}{dp}\right)_H\right)} \quad , \quad (3.4)$$

where $\left(\frac{du}{dP}\right)_H$ is the total derivative along the partial reaction Hugoniot curve corresponding to $\lambda_1 = 1$ and $\lambda_i = 0$. As before, we assume that the fluid ahead of the shock is quiescent and the reaction rates there are zero. Equation (3.4) is an ordinary differential equation involving the two dependent variables [P] and $\left[\frac{\partial u}{\partial h}\right]$. Since $\left[\frac{\partial u}{\partial h}\right]$ is not known a priori we must also formulate an equation for it. Equations (2.21) and (2.24) serve as the starting point for such a development. In place of Eq. (2.22) we need the analogous expression for a reactive fluid. Taking the partial derivative with respect to time of Eq. (3.3) and then applying the jump conditions gives

$$2U\frac{dA}{dt} + A\frac{dU}{dt} = \frac{d^2[P]}{dt^2} + \left(\rho_o^2 U^2 - z^2\right)\left(\frac{J}{\rho_o^2}\right) + \left(\frac{\partial z^2}{\partial v}\right)_S \left(\frac{B}{\rho_o}\right)^2$$
$$+ \frac{1}{E_p^2}\left[\sum_{i=2}^{n} q_i r_i\right]\left(2\left(\frac{\partial E_p}{\partial v}\right)_S + 1\right)\frac{B}{\rho_o} - \frac{1}{E_p}\left[\sum_{i=2}^{n} q_i \frac{\partial r_i}{\partial t}\right]$$
$$+ \frac{E_{pp}}{E_p^3}\left[\left(\sum_{i=2}^{n} q_i r_i\right)^2\right] \quad , \quad (3.5)$$

where $J \equiv \left[\frac{\partial^2 P}{\partial h^2}\right]$. Again we find that an additional unknown, J, has been introduced. Continuing this procedure (i.e., deriving an equation for J) only leads to more new unknowns $\left[\frac{\partial^3 P}{\partial h^3}\right]$ being introduced, and eventually leads to the creation of an infinite hierarchy of differential equations.

If the flow at the high-pressure side of the discontinuity is sonic, then the equations uncouple. Since we require [P] to be bounded, $\left[\sum_{i=2}^{n} q_i r_i\right]$ must be equal to zero. There are a number of ways that this can be achieved. A single reversible chemical reaction which is at equilibrium at the discontinuity satisfies the above condition. Wood and Parker[28] have shown that the slope at the discontinuity decreases more rapidly with time than it does for a nonreactive fluid and that at long times (compared with the relaxation time) a growing region of constant state develops behind the frozen sonic point. Another possibility is two irreversible reactions of opposite thermicity, whose rates at the sonic point are adjusted so that $q_2 r_2 + q_3 r_3 = 0$. Two different types of behavior are possible depending on whether the system is basically endothermic $q_2 + q_3 < 0$ or exothermic $q_2 + q_3 > 0$. For the endothermic case the slope A reaches a steady state positive value corresponding to the establishment of a steady weak detonation. For the exothermic case A decreases until at some finite time it approaches negative infinity at which time a shock develops, thereby restoring the coupling between Eqs. (3.4), (3.5), etc.

Although the assumption of sonic flow at the shock simplifies the analysis of Eqs. (3.4), (3.5), etc., it restricts [P] to be constant. Since our aim is to construct a model which allows [P] to increase with run we must proceed differently. For the sake of simplicity we limit our discussion to the following constitutive relations: one irreversible slow kinetic step obeying Eq. (2.37), and a polytropic equation of state

$$E = \frac{Pv}{\gamma - 1} - q\lambda_1 + q_2(\lambda_1 - \lambda_2) \quad , \quad (3.6)$$

where $q_2 > 0$ and γ is a free adjustable parameter. The assumption that the first reaction occurs instantaneously places the detonation wave on the $\lambda_1 = 1$, $\lambda_2 = 0$ Hugoniot curve. Specifying any one of the variables [P], [ρ], [u], or U on this Hugoniot curve determines the others. If we take the CJ point of the detonation with energy release q_1 as a reference point (the asterisk being used to denote this reference state), and define

$$\varepsilon \equiv \frac{[P]}{P^*} - 1 \tag{3.7a}$$

then

$$[u] = u^*(1 + 2\varepsilon)^{\frac{1}{2}} \tag{3.7b}$$

$$[\rho] = \rho^* \frac{(1 + \varepsilon)}{\left(1 + \frac{\gamma-1}{\gamma}\varepsilon\right)} - \rho_o \tag{3.7c}$$

$$U = D^* \frac{(1 + \varepsilon)}{(1 + 2\varepsilon)^{\frac{1}{2}}} \quad , \tag{3.7d}$$

where we have assumed that u and P in the unshocked material are zero and

$$P^* = \frac{\rho_o D^{*2}}{\gamma+1} \tag{3.8a}$$

$$u^* = \frac{D^*}{\gamma+1} \tag{3.8b}$$

$$\rho^* = \rho_o\left(\frac{\gamma+1}{\gamma}\right) \quad . \tag{3.8c}$$

The total differential of any of these variables along the Hugoniot curve is directly related to $d\varepsilon$ through Eqs. (3.7). At this point it is convenient to introduce the scaled variables

$$\delta = (q_2/q_1)^{\frac{1}{2}} \tag{3.9a}$$

$$t' = \delta k_2 t \tag{3.9b}$$

$$U' = U/D^* \tag{3.9c}$$

$$A' = (D^*/k_2 P^*)A \tag{3.9d}$$

$$J' = (D^{*2}/k_2{}^2 P^*)J \tag{3.9e}$$

$$B' = (\rho_o D^{*2}/P^* k_2)B \tag{3.9f}$$

$$z' = z/(\rho_o D^*) \quad . \tag{3.9g}$$

Written in terms of these variables Eqs. (3.4) and (3.5) become (dropping the primes)

$$\delta\frac{d\varepsilon}{dt} = -\tfrac{1}{2}\left(\frac{\rho}{\rho_o}\right)\left(\frac{1+2\varepsilon}{2+3\varepsilon}\right)\left(\frac{2\varepsilon(1+\varepsilon)}{(1+2\varepsilon)}B - \delta^2\right) \tag{3.10}$$

$$2\delta U\frac{dA}{dt} + \delta A\frac{dU}{dt} = \delta^2\frac{d^2\varepsilon}{dt^2} - \frac{\rho}{\rho_o}\frac{\varepsilon(1+\varepsilon)}{(1+2\varepsilon)}J - \left(\frac{\gamma}{\gamma+1}\right)\left(\frac{\rho}{\rho_o}\right)^2\left(1+\varepsilon\right)B^2 + \tfrac{1}{2}\left(\frac{\rho}{\rho_o}\right)^2\delta^2 B + \tfrac{1}{4}\left(\frac{\rho}{\rho_o}\right)\delta^2 \quad , \tag{3.11}$$

where ρ/ρ_o and U are given by Eqs. (3.7c) and (3.7d) and A and B are related by Eq. (2.24). Progress can be made at finding a solution to these coupled equations by taking advantage of the smallness of the energy fraction δ. A simple perturbation expansion in δ of the solution of this set reduces the problem to more managable proportions. It is a simple matter to show that

$$\varepsilon = O(\delta) \tag{3.12a}$$

$$A = O(\delta), \; B = O(\delta) \tag{3.12b}$$

$$J = O(\delta^2) \tag{3.12c}$$

$$U = 1 + O(\delta^2) \quad , \tag{3.12d}$$

where we assume expansions of the form

$$\varepsilon(t) = \delta\varepsilon_1(t) + \delta^2\varepsilon_2(t) + \cdots \tag{3.13}$$

for all of the dependent variables. Substituting these expansions into Eqs. (3.10), (3.11) and retaining only highest order terms gives

$$\frac{d\varepsilon_1}{dt} = \left(\frac{\gamma+1}{4\gamma}\right)\left(1 - 2\varepsilon_1 B_1\right) \tag{3.14a}$$

$$\frac{dB_1}{dt} = \tfrac{1}{2}\left(\frac{\gamma+1}{4\gamma}\right)\left(1 - 4B_1{}^2\right) \quad . \tag{3.14b}$$

If we assume that initially $\varepsilon = 0$ and $\lim_{t \to 0} B \to \infty$ the solution to these equations is

$$B_1 = \tfrac{1}{2}\coth\tau \tag{3.15a}$$

$$\varepsilon_1 = \tanh(\tfrac{1}{2}\tau) \quad , \tag{3.15b}$$

where

$$\tau \equiv \left(\frac{\gamma+1}{4\gamma}\right)t \quad . \tag{3.16}$$

Equations (3.15a) and (3.15b) give the pressure and slope $\frac{\partial u}{\partial h}$ at the shock to first order in the smallness parameter δ. Since J and all higher order derivatives are of higher order in δ, these equations represent the complete solution to order δ. What these solutions show is that the pressure on the $\lambda_1 = 1$,

$\lambda_2 = 0$ Hugoniot curve increases from an initial value of P* to a final steady value that is greater than this value ($q_2 > 0$). The time required to reach 90% of the steady-state value of [P] - P* is of order (10/δ) reaction times. For early times the slope begins by being equal to the value for a Chapman-Jouguet detonation in a γ-law fluid and for late times it approaches a constant steady value which is characteristic of the steady-state two-reaction ($q_1 > 0$, $q_2 > 0$) detonation. This slope is always greater than or equal to that of the γ-law Taylor wave in the Chapman-Jouguet detonation.

Figures 3.1a and 3.1b show the early and late time behavior for our two-reaction model. At early times the first reaction is nearly frozen and the flow behaves much as a Chapman-Jouguet detonation with a pressure P*. At very late times the reaction zone structure becomes apparent with the pressure on

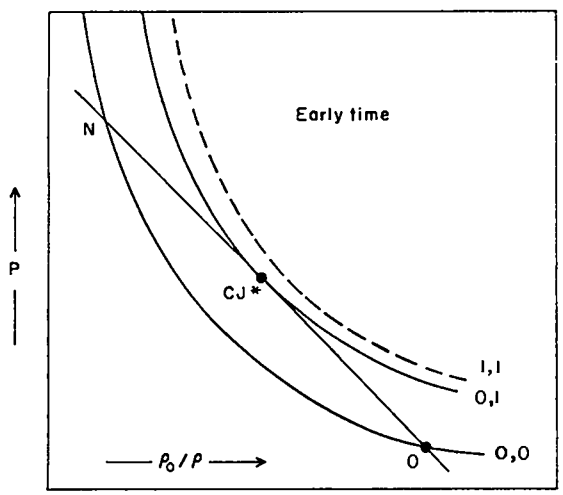

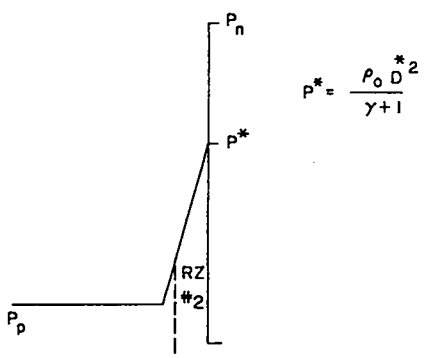

Fig. 3.1a A schematic representation of the early time behavior of our time-dependent detonation model.

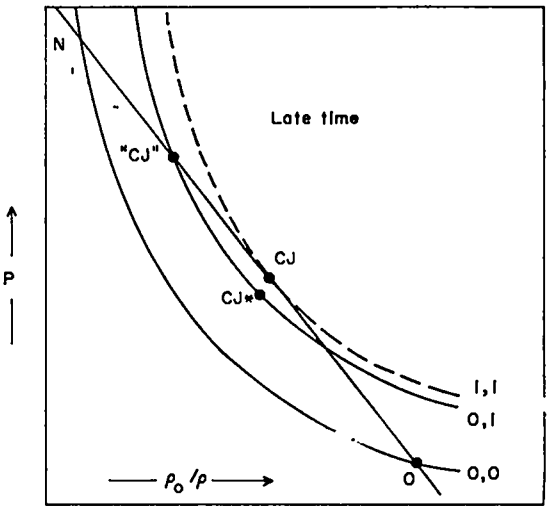

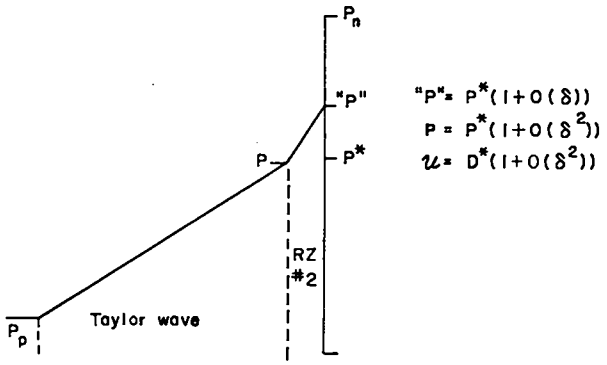

Fig. 3.1b A schematic representation of the late time behavior of our time-dependent detonation model.

the $\lambda_1 = 1$, $\lambda_2 = 0$ Hugoniot increasing to "P" = P* [1 + $O(\delta)$] while the pressure at the sonic plane remains nearly equal to the initial value $P = P^*[1 + O(\delta^2)]$. If the second reaction zone is reasonably large then the pressure "P" is the value inferred from free-surface velocity measurements. Therefore, we have shown that by including a second slow exothermic process in our detonation model we can at least qualitatively account for both the steep slope of the free-surface velocity curves for large charges and the increase in the apparent Chapman-Jouguet pressure "P" with run.

For purposes of calculation we need to include higher order terms (in δ) in our shock jump relations.

To do this additional equations must be added to our system, in particular an equation for J if we are to go up to order δ^2. Proceeding as we did in the derivation of Eq. (3.11) we readily obtain

$$\frac{dJ_2}{dt} + \frac{3}{2}\left(\frac{\gamma+1}{\gamma}\right) A_1 J_2 = \tfrac{1}{2}\frac{d^2A_1}{dt^2} + \frac{1}{\gamma}\left(\frac{\gamma+1}{2\gamma}\right)A_1\left(\tfrac{1}{4} - A_1^2\right) , \tag{3.17}$$

where J_2 is the leading term in J. This equation is easily solved yielding

$$J_2 = \left(\frac{\gamma-1}{8\gamma}\right) \operatorname{csch}^2\tau \quad . \tag{3.18}$$

Using this result we can go on and obtain the second order corrections to ε and B

$$B_2 = -\left(\frac{\gamma+1}{4\gamma}\right) \tanh\left(\tfrac{1}{2}\tau\right) \tag{3.19}$$

$$\varepsilon_2 = \varepsilon_1^2 + \left(\frac{7\gamma-3}{4\gamma}\right) \operatorname{sech}\left(\tfrac{1}{2}\tau\right) \left[\operatorname{sech}\left(\tfrac{1}{2}\tau\right) - \tfrac{1}{2}\tau \operatorname{csch}\left(\tfrac{1}{2}\tau\right)\right] \quad . \tag{3.20}$$

Using Eqs. (3.15), (2.28), (2.29) and Fig. 2.5 it is possible to get a good estimate of the parameter values (γ, D^*, δ, k_2) needed to reproduce both the intercepts and the initial slopes of the Composition B/dural experiments. However, the calculations on other experiments would be prohibitively difficult without the aid of a one-dimensional hydrodynamic code. In the next section we discuss the numerical solution of the hydrodynamic equations for our model obtained by using a Lagrangian mesh code.

IV. NUMERICAL SOLUTION OF THE FLOW EQUATIONS

A. Programming the Shock

All of the numerical solutions of the partial differential equations describing our model were obtained with the one-dimensional Lagrangian mesh code PAD3.[29] The differencing scheme used by this code employs a net on which all variables are centered in time and the pressure, density, internal energy, and composition are cell-centered quantities while the position and particle velocity are those of the right cell boundary. Before any calculations could be performed a simple modification of the code had to be made.

We recall that our two-reaction detonation model assumes that the relaxation time for the first reaction is many orders of magnitude shorter than that of the second reaction. The disparity in times makes it impossible to resolve the very fast reaction zone and still retain a sufficient number of mesh cells for the remainder of the reactive flow and the Taylor wave. This difficulty can be circumvented if the first reaction zone is replaced by a sharp shock burn, thereby leaving the entire mesh for the second reaction zone and the Taylor wave. A special programmed shock advance package written by Wildon Fickett and Jack Jacobson[30] was used to accomplish this. The basic operational plan of the programmed shock advance calls for the replacement of the smeared shock and fast reaction zone by an operator-controlled sharp shock rise to a prescribed state on the ($\lambda_1 = 1$, $\lambda_2 = 0$) Hugoniot curve. Figure 4.1 shows a schematic representation of four adjacent mass cells in our Lagrangian mesh at time t. At this time, cell i + 2 is quiescent and at the original density ρ_o, while cell i + 1 contains the programmed shock. The shock is advanced a distance $U(t)\Delta t$ every time step (Δt), with Δt adjusted so as to both guarantee computational stability and fix the transit time of the shock across the cell at an integral number of time steps

$$\Delta t = \frac{\Delta\zeta_o}{4U(t)} \quad , \tag{4.1}$$

where $\Delta\zeta_o$ is the original cell dimension and $U(t)$ is

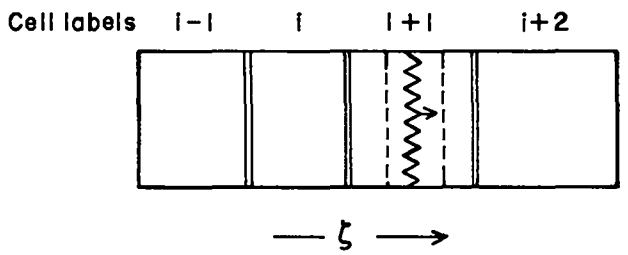

Fig. 4.1 A schematic representation of four mass cells (particles) in our Lagrangian mesh calculation at time t. The cell i + 2 is quiescent, i + 1 contains the programmed shock (ξ), i has a programmed right boundary velocity, pressure, density, and internal energy, and i - 1 is an ordinary mesh cell in the calculation. In this example the shock traverses cell i + 1 in four time steps (currently at step two).

held constant in each cell but may vary from cell to cell. To produce the desired compression associated with the passage of the shock, the right boundary of cell i is advanced at the particle velocity on the ($\lambda_1 = 1$, $\lambda_2 = 0$) Hugoniot curve, [u]. When the shock arrives at the right boundary of cell i + 1, the density of this cell at that time is given by

$$\rho_{i+1} = \rho_o \left(1 - \frac{[u]}{U}\right)^{-1} , \qquad (4.2)$$

while the pressure and internal energy are given by their respective shock conservation conditions. The "snapshot" shown in Fig. 4.1 has cell i with its right boundary velocity, pressure, density, and composition programmed at the values [u], [P], $[\rho]+\rho_o$, and ($\lambda_1 = 1$, $\lambda_2 = 0$) respectively. Therefore, it is the cell whose state corresponds to the high-pressure side of the shock discontinuity between the ($\lambda_1 = 0$, $\lambda_2 = 0$) and ($\lambda_1 = 1$, $\lambda_2 = 0$) partial reaction Hugoniots. The evolution of cell i - 1 and all of its neighbors to the left is controlled by the standard mesh code integration, subject to the boundary conditions being imposed in cell i and at the left boundary of our system plus the initial conditions. As time passes the special cell designation is advanced to cell i + 2, etc.

It is important that the specification of cell i's state be as consistent as is possible if the amount of numerical noise in these calculations is to be kept to a minimum. If the time-dependent $0(\delta^2)$ jump conditions derived in the previous section are used to set the state of cell i, the perturbations introduced by imperfections in the shock jump conditions will be minimized. Figures 4.2 show the particle velocity vs distance profiles generated using the sharp shock burn and PAD3. The parameter values used in the reaction zone are those describing Composition B (see Sec. V) while a JWL equation of state as calibrated by Rivard[19] (JWLR) was used for the isentropic release wave. These "snapshots" show the final form of the detonation wave profiles that develop in explosive charges which are approximately 50-mm, 100-mm, and 200-mm long. Since as a general rule the quality and accuracy of a calculation depends to a large measure on the number of mesh cells used per unit particle velocity gradient, 512 cells were used in each of the above calculations. Owing

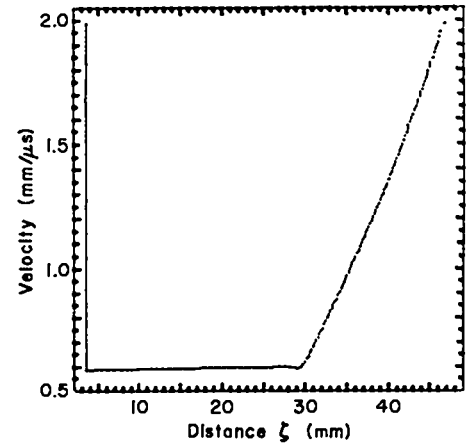

Fig. 4.2a

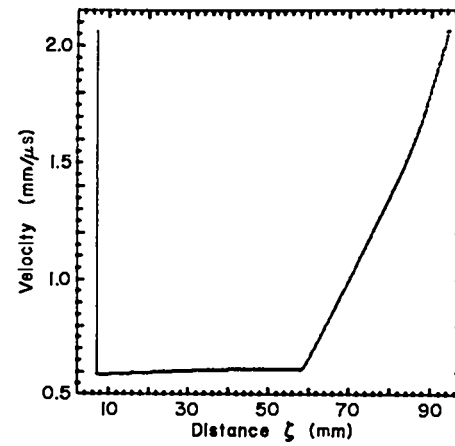

Fig. 4.2b

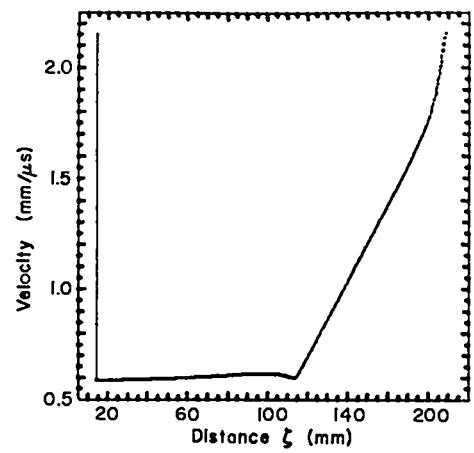

Fig. 4.2c

Figs. 4.2 The computer-generated particle velocity vs distance (ζ) profiles for our two-reaction detonation model. The parameters used in the reaction zone are those describing Composition B ($D^* = 7.85$ mm/μs, $\gamma = 3.15$, $\delta = 0.16$, $k_2 = 2\ \mu s^{-1}$, $\rho_o = 1.73\ Mg/m^3$).

to the non self-similar nature of the flow, this does not lead to strictly equivalent calculations. Nevertheless, if we disregard this difference it is clear that the overall quality of each of the wave profiles is good and comparable to the others. Momentarily returning our attentions to the physical aspects of the problem, we see that the passage of time brings with it the development of a reaction zone profile which is distinct from that of the Taylor wave, and in keeping with the results of experiments.

The wave profiles shown in Fig. (4.2) were all obtained by solving a set of difference equations for the model and not the partial differential equations themselves. Presumably, if the mesh were made finer and finer the solutions of the difference equations would approach the solutions of the parent differential equations. Unfortunately, the computation time increases as the square of the number of mesh cells. Therefore, as a practical matter one would like to use as few cells as possible and yet be able to obtain, by extrapolation if necessary, solutions of high quality. Although the number of cells necessary to get acceptable numerical errors for such experiments as the integrated motion of embedded foils in a piece of explosive (as well as the other less sensitive experiments) is not large, an accurate calculation of the explosive-induced free-surface velocity of an inert plate requires substantially more cells.

B. Accuracy of the Difference Equation Solutions

The calibration of our time-dependent detonation model and in fact the very need for such a model is based on the inability of the Chapman-Jouguet theory to reproduce free-surface velocity measurements. It is for this reason that we now examine the numerical solution to the explosive/inert interaction problem with a special interest in achieving high accuracy with a minimum number of computational cells. For the purposes of this study we use 25 mm of the following ideal (Chapman-Jouguet) explosive

$$\rho_o = 1.84 \text{ Mg/m}^3 \tag{4.3a}$$

$$D = 8.8 \text{ mm/}\mu\text{sec} \tag{4.3b}$$

$$\gamma = 3.276 \tag{4.3c}$$

and a constant-γ equation of state. The explosive burn is via the Hot Start option in PAD3. As in the programmed burn discussed earlier this burn also generates a sharp shock detonation wave thus making it ideal for our purposes. The calculations involving the inert are somewhat different. Since we choose to have the code generate the shock there, this requires that an artificial viscosity be added to the calculation. In our work we use the Landshoff[29] form of the artificial viscosity, with the multiplier selected so that our shock waves are neither strongly overdamped nor underdamped.

Our chief concern with inerts and the explosive/inert interaction is the calculation of the initial free-surface velocity of these plates. Given an equation of state for the inert, the initial free-surface velocity of a plate of thickness x can be calculated once the particle velocity at the head of shock (u_s) located at x is known. If the description of the inert is via a Walsh equation of state, we simply have

$$U_{fs} = 2u_s \quad . \tag{4.4}$$

For any other perfect fluid equation of state

$$U_{fs} = u_s + \int c \, d\ln\rho \quad , \tag{4.5}$$

where the Riemann integral is to be performed along the release isentrope of the inert. Tables giving $U_{fs}(u_s)$ for inerts characterized by a Mie-Grüneisen equation of state are available.[31] The simplicity of the conversion between u_s and U_{fs} is especially convenient because it allows one to calculate the entire $U_{fs}(x)$ curve from one explosive/inert calculation. Now $u_s(x)$ can be obtained from the standard PAD3 output in two different ways. The more conventional of these is simply to locate the mesh cell with the maximum particle velocity at some time and record its position and particle velocity as those of the shock (reading the cycle prints). In addition to this method, a Shock Save routine is available which assigns the value of x for which the artificial viscosity is a maximum as the position of the shock, and $u_s(x)$ by linearly extrapolating the following rarefaction to this point. Figure 4.3 is a schematic representation of these two methods for a shock followed by a rarefaction wave. The smearing of the wave front by the viscous forces is apparent. Reading the cycle print, one tends to underestimate the value at the shock, while the Shock Save, which is

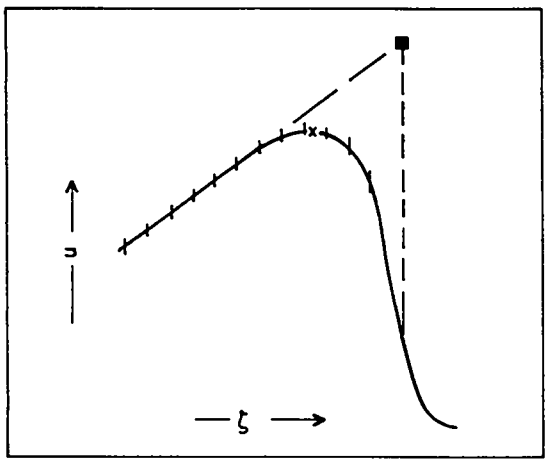

Fig. 4.3. A schematic representation of a shock and following rarefaction in an inert. The ticks represent cell boundaries, and (x) denotes the particle velocity maximum while (■) is obtained from Shock Save.

an attempt to remove the effects of viscosity, probably overestimates the value.

The overall quality and value of code-generated results depends in large measure on such parameters as the magnitude of the artificial viscosity in the inert and the number of mesh cells used in the calculation. Particularly important is the selection of a viscosity multiplier for the inert. In general, the optimal value is not constant but changes in going from one inert to another. The optimization of the calculation with respect to the viscosity multiplier can most conveniently be carried out by studying the viscosity dependence of a square-topped shock. Figures 4.4 show the history of a mass cell in PMMA (LA-4167-MS) which has been shocked up to pressures typical of those produced by the interaction of an explosive with a low impedance inert. The Landshoff viscosity multiplier assumes the values 0.5, 0.75, and 1.0 in these calculations. Examination of these figures clearly shows that a value of 0.75 is the best choice for PMMA, since it produces a shock which is neither strongly underdamped (0.5) nor overdamped (1.0). Optimization of the viscosity multiplier value is considerably more important for the wave shown in Fig. 4.4 than for the square-topped shock. Clearly if the oscillations characteristic of an underdamped shock are present in the calculation, neither the cycle print nor the Shock Save will be of any value. Proceeding in a similar fashion for a higher impedance inert (dural, LA-4167-MS) we find that the somewhat lower value of 0.5 is more satisfactory for the viscosity multiplier.

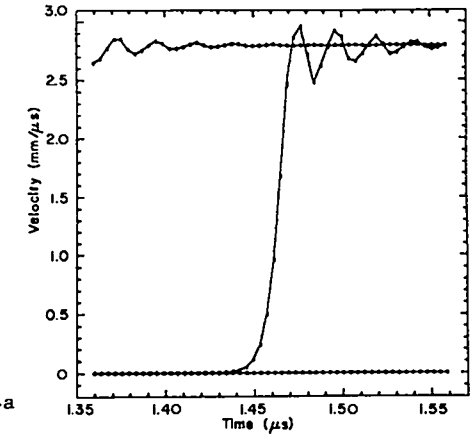

Fig. 4.4a

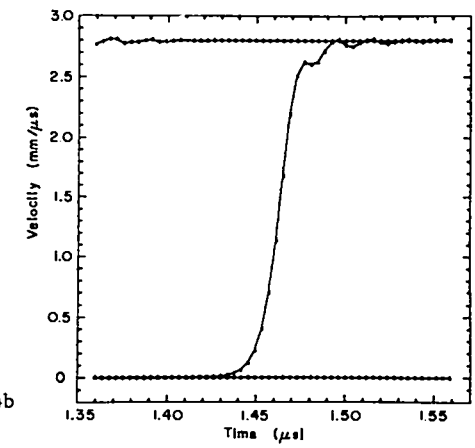

Fig. 4.4b

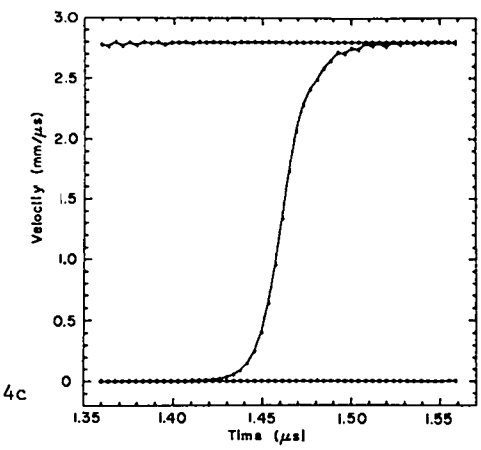

Fig. 4.4c

Fig. 4.4. The history of a particle in shocked PMMA calculated using a Landshoff viscosity. The viscosity multiplier is set at 0.5 (underdamped), 0.75 (neutral), and 1.0 (overdamped) in Fig. 4.4a,b, and c respectively.

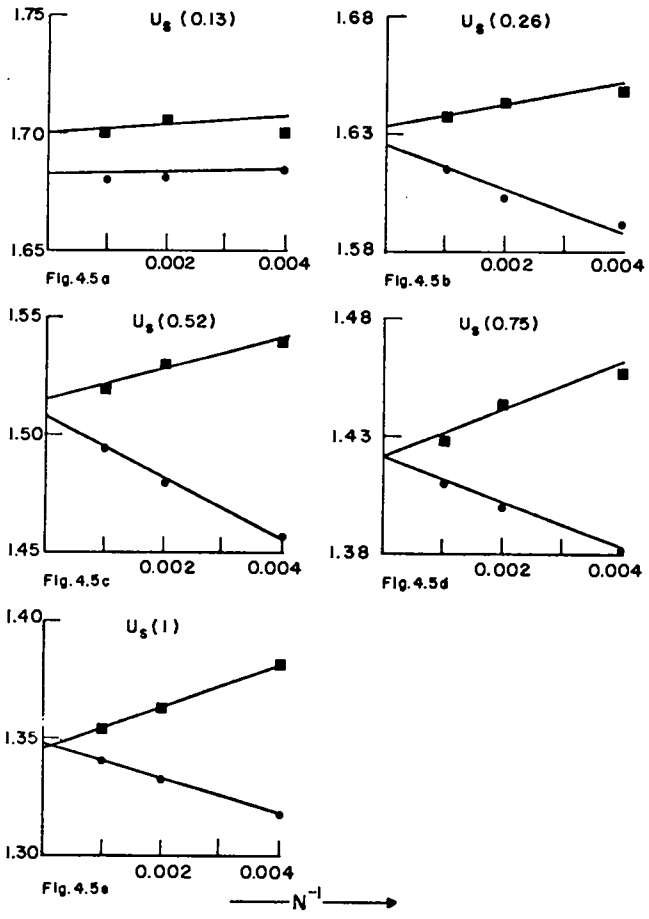

Fig. 4.5 The dependence of $u_s(x/X)$ in dural on mesh size and output routine.

● cycle print ■ Shock Save

Having selected optimal values for the viscosity multipliers we turn our attention to the effect of mesh size on the quality of our calculation. The problem we examine consists of 25 mm of the ideal explosive described by Eq. (4.3) driving 25 mm of dural. A comparison is made of both output routines for systems with a total of 250, 500, and 1000 mesh cells. In each case the values of $u_s(x)$ obtained from the code were smoothed. Figure 4.5 shows $u_s(x/X)$ vs the reciprocal of the total number of cells in the system (N^{-1}) for various values of the ratio x/X, where X is the length of the explosive. It shows that the Shock Save output is consistently above that obtained from the cycle print and, except for the shortest plate (x/X = 0.13), both extrapolate to the same intercept for an infinite number of cells. The failure of the extrapolation for x/X = 0.13 is probably a result of the considerable amount of noise at the explosive/inert interface that is characteristic of the Hot Start explosive burn. Interpreting the infinite N intercepts as the solution of the governing differential equations, we find that reading either of the output routines without proper extrapolation will produce unacceptably large errors in the free-surface velocities. However, if an average of the output from the cycle print and Shock Save is taken, any reasonable number of cells ($N^{-1} < 0.005$) will yield the sought-after solution. The excessive calculation noise for small values of x/X can easily be overcome. Since $u_s(x)$ is a smooth function of x a good value for $u_s(0)$ can be obtained by extrapolation. Doing such an extrapolation we get $u_s(0) = 1.773$ mm/μs as compared to the calculated interface match $u_s(0) = 1.776$ mm/μs. The results obtained here for 25 mm/25 mm of explosive/dural are of course valid for any size system with the same x/X and total number of cells.

A similar set of calculations for PMMA, using 0.75 as a viscosity multiplier, gives results identical to those for dural. From the results obtained here we conclude that the best value to use for $u_s(x)$ is the average of the cycle print and Shock Save outputs. In the free-surface velocity calculations that we report in the following sections this prescription is used.

C. Equation of State of the Inert

All of the explosive/inert calculations that we have considered to this point have assumed that the inert behaved as a perfect fluid. It is well known that materials such as dural also have an elastic contribution to the total stress. Although the discussion of such a phenomenon may be somewhat out of place in a section devoted to the numerical solution of differential equations, we will briefly examine the importance of material strength on our free-surface calculations. The elastic, perfectly plastic model of Von Mises[32] will be used to describe the inert.

In Sec. II. B we mentioned that because elastic unloading proceeds more rapidly than the hydrodynamic unloading, adding material strength to our calculation has the effect of increasing the sound velocity in the rarefaction. This increase in the sound velocity at the shock leads to a steeper $u_s(x)$ vs x curve. Using 25 mm of the ideal explosive of Eq. (4.3) as a driver we calculate and compare the free-surface velocities produced in purely plastic

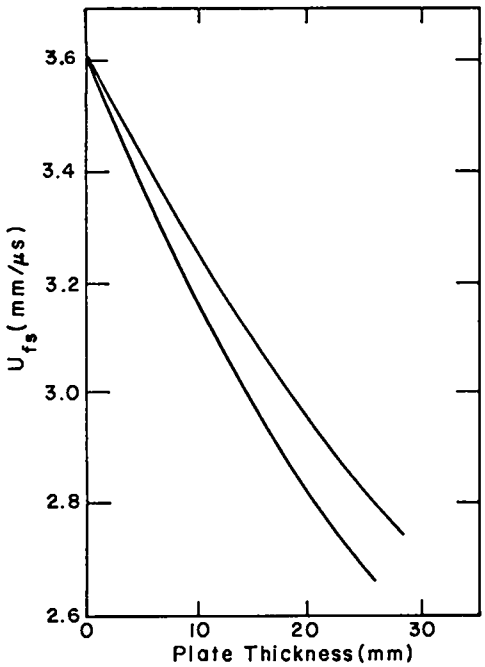

Fig. 4.6. The free-surface velocity induced into purely plastic (upper) and elastic-plastic (lower) dural by the ideal explosive of Eq. (4.3).

dural (LA-4167-MS) and elastic, perfectly plastic dural. The dural hydrostat is obtained by subtracting the elastic component from the experimental Hugoniot curve (LA-4167-MS). A value of 0.3 GPa is taken for the yield strength and 25 GPa for the shear modulus. The results of these calculations are shown in Fig. 4.6. They clearly show that for the 25-mm explosive charge used in these calculations the slope of U_{fs} vs x is considerably steeper when material strength is included.[10] Although the differences will not be as great for larger explosive charges as for the example considered here, it seems clear that in materials with strength, elastic-plastic effects must be included if a realistic free-surface velocity calculation is to be made.

V. TIME-DEPENDENT DESCRIPTION OF COMPOSITION B

A. Calibrating the Model

The calibration of our time-dependent model involves selecting values for the four parameters D^*, γ, δ, and k_2. This was done by fitting the $0(\delta^2)$ expressions for [u] and $[\frac{\partial u}{\partial h}]$ matched from the explosive into the dural, to the data shown in Fig. 2.5. These data include both intercept and initial slope information at four different charge lengths. In performing the calibration we take advantage of the facts that to $0(\delta)$

$$[\frac{\partial u}{\partial \zeta}] = \frac{\delta k_2}{2\gamma} \coth \left[\left(\frac{\gamma+1}{4\gamma}\right) \delta k_2 t\right] + 0(\delta^2) \qquad (5.1)$$

contains the parameters δ and k_2 only as δk_2 (we have returned to dimensioned variables), and that the impedance match of $u_s(0)$ back into the explosive neither depends strongly on the value which the constant γ assumes nor on small deviations in $U(t)$ of the order of a few hundred m/s. Beginning with $\gamma = 3.0$ and $U(t) = 7.9$ mm/μs, the four values of $u_s(0)$ are matched into the explosive yielding the corresponding values [P], [u], etc. In turn, these values are used to calculate the required unknowns in Eqs. (2.28) and (2.29). Combining these equations with Eq. (5.1), the nonlinear least squares routine PACKAGE[33] is used to fit δk_2 to the experimental values of $\frac{dU_{fs}}{dx}\Big|_{x=0}$. Substituting the $0(\delta^2)$ expressions for [P] and $U(t)$ into the impedance match equation, δ and γ are fit (while δk_2 is held fixed) so as to get the best agreement with the intercept values $u_s(0)$. These values for δ and γ allow us to get reasonable estimates for D^* and k_2. The entire procedure is then repeated, now using the $0(\delta^2)$ expression for $[\frac{\partial u}{\partial \zeta}]$, until a set of parameters (D^*, δ, γ, k_2) is obtained which is judged to be acceptable. Using these values of the parameters in our time-dependent explosive burn, the PAD3 code is used to calculate the dural free-surface velocity curves. The calculated and experimental curves are then compared; if any changes in the parameters are suggested by this comparison they are made.

The entire fitting procedure is then repeated (holding the selected parameter fixed) until results of the desired quality are obtained. Proceeding as outlined above we find that

$$D^* = 7.85 \text{ mm/μs} \qquad (5.2a)$$

$$k_2 = 2.0 \text{ μs}^{-1} \qquad (5.2b)$$

$$\gamma = 3.15 \qquad (5.2c)$$

$$\delta = 0.160 \qquad (5.2d)$$

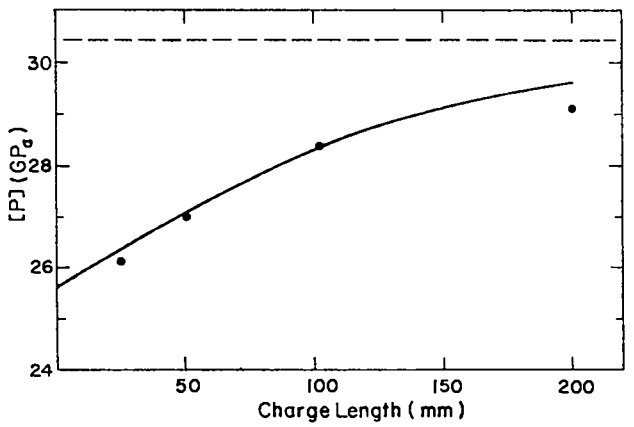

Fig. 5.1. The apparent "Chapman-Jouguet pressure" [P] vs the charge length for Composition B. The dashed line represents the infinite medium asymptote, while ● represents the pressures corresponding to the data on Fig. 2.5.

provide a reasonable fit to all of the dural free-surface velocity data. The constants of Eq. (5.2) were obtained by using the turbulence model[27] in place of the reactive fluid model discussed in Sec. III. However, since the differences between these two models are not large for the calculations that we will report, the results we obtain apply equally well to either a slow chemical or slow physical exothermic second rate process. Figure 5.1 shows the apparent "Chapman-Jouguet pressure" [P], calculated with the $O(\delta^2)$ shock jump condition, as a function of the charge length (time). The agreement between the fit function and the data (●) is good.

B. Calculated Free-Surface Velocities

The real test is of course how well our model reproduces the measured free-surface velocities. Using the calibration given by Eq. (5.2) we obtain the results shown in Fig. 5.2. The agreement between calculation and experiment is excellent. It is clear that the Chapman-Jouguet theory, even after calibration to the appropriate intercept, reproduces the observed data only for charge lengths less than or equal to 50 mm. Therefore, we find that unlike the Chapman-Jouguet theory, our time-dependent model is consistent with the data used in its calibration. Considering the simplicity of our model (constant-

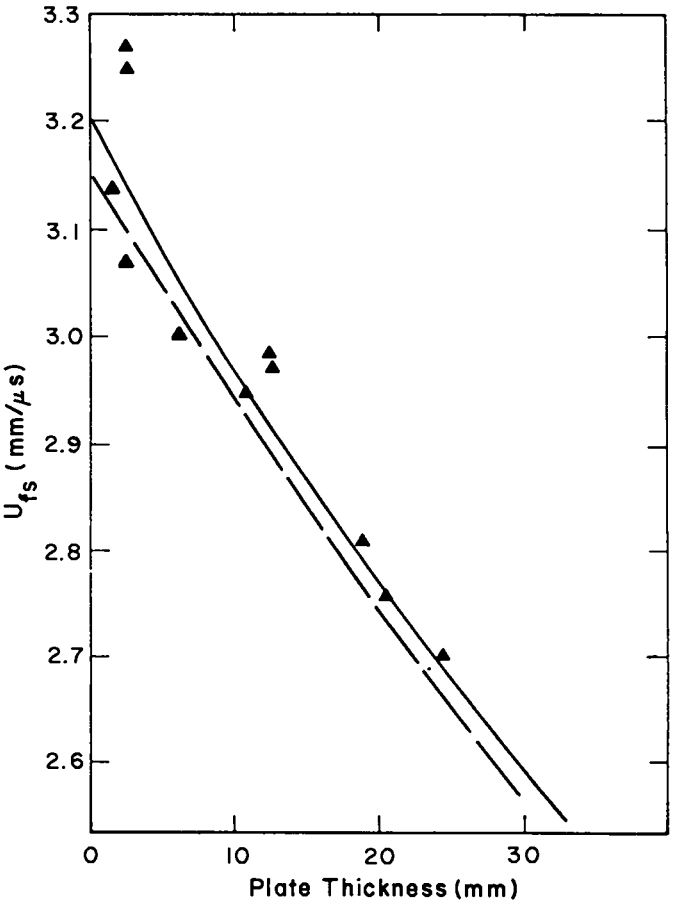

Fig. 5.2a. The free-surface velocity of dural plates induced by a 50.8-mm charge of Composition B.

Elastic-plastic dural
Hydrostat; LA-4167-MS
Yield Strength;[23] 0.3 GPa
Shear Modulus;[23] 25 GPa
Our model ————————
Composition B of Eqs. (5.2)
Chapman-Jouguet Model —— ——
ρ_o = 1.73 Mg/m^3, D = 7.85 mm/μs,
γ = 2.98
The data ▲

γ reaction zone, simple decay law, etc.) the agreement is remarkably good.

A limited amount of data is also available for 76 mm of Composition B (X/d = 1) driving perfectly plastic 1100F Al (LA-4167-MS). These data are interesting because they were obtained using a pin technique (Warnes[34]). Since our model was calibrated to Deal's measurements, this result suggests that the values obtained with the pin technique are in excellent agreement with Deal's technique.

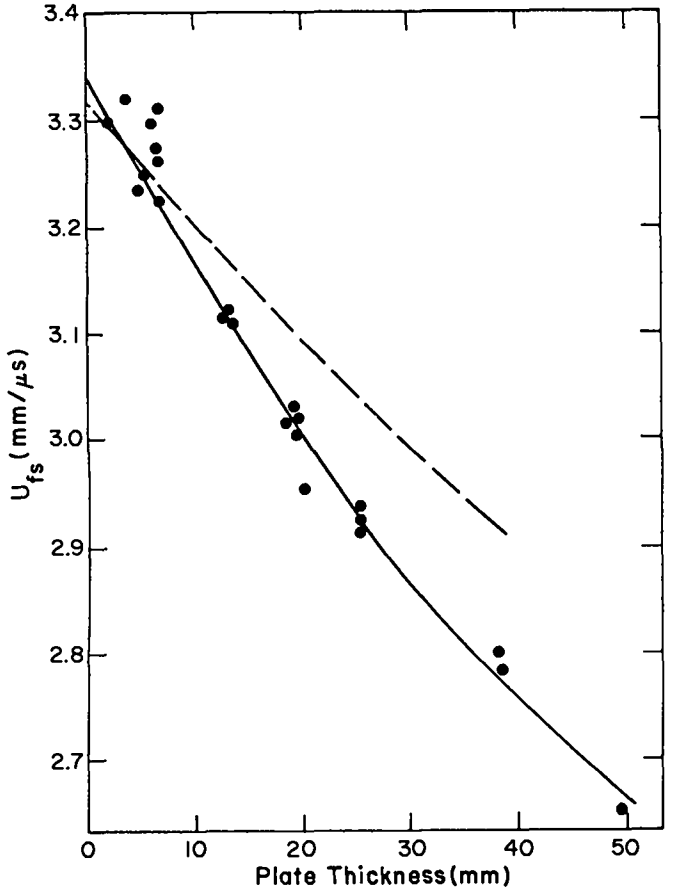

Fig. 5.2b. The free-surface velocity of dural plates induced by a 101-mm charge of Composition B.

Dural Fig. 5.2a
Our model ————————
Chapman-Jouguet model —— ——
ρ_o = 1.73 Mg/m^3, D = 7.85 mm/μs, γ = 2.76
The data ●

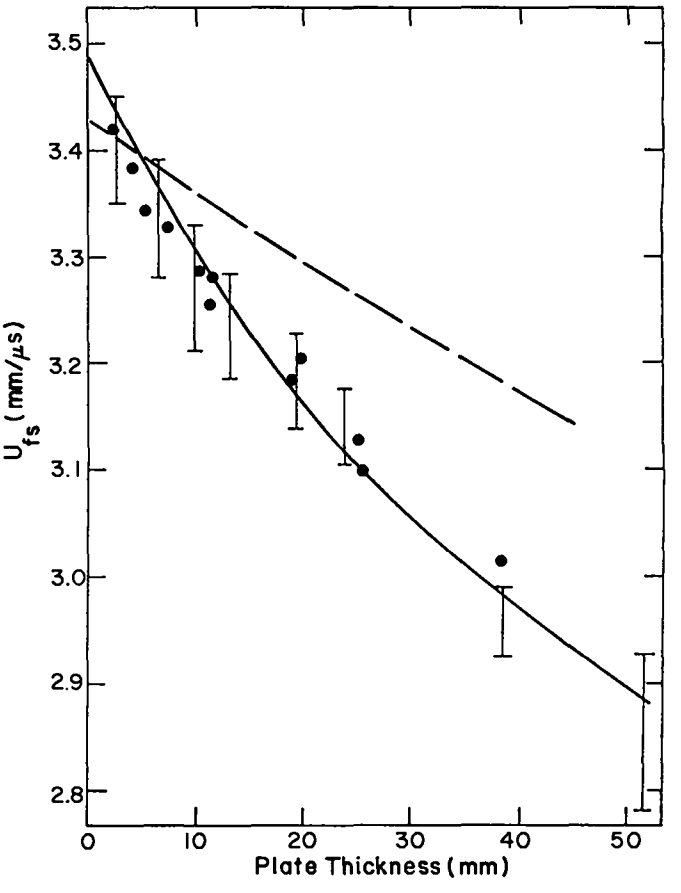

Fig. 5.2c. The free-surface velocity of dural plates induced by a 203-mm charge of Composition B.

Dural Fig. 5.2a
Our model ————————
Chapman-Jouguet model —— ——
ρ_o = 1.73 Mg/m^3, D = 7.85 mm/μs, γ = 2.64
The data ●, I

In a series of experiments designed to measure the reflected shock Hugoniot curve of the "reactive products" of Composition B, Deal[12] measured the free-surface velocities of a number of other inerts. These experiments, which were performed using a 203-mm-long charge of Composition B as a driver, provide us with $U_{fs}(x)$ for inerts ranging from Plexiglas to uranium. This spectrum of inerts gives us a range of shock properties which is sufficient to noticeably expand and contract the image of the reaction zone in the inert. For example, Deal's uranium data probe the flow well beyond the reaction zone. Figure 5.3 compares our calculation with the experimental data. Examination of this figure shows that the slope of the experimental data changes at about 15 mm of plate thickness. Comparing our calculated curve to this data we find the agreement to be good. The break in the calculated curve is a result of the change in slope in going from the reaction zone to the Taylor wave. Considering that the location of this break is determined by the calibration of our model to the $U_{fs}(0)$ and $\frac{dU_{fs}(0)}{dx}$ data for dural, the agreement with this data is indeed good. These data are also valuable

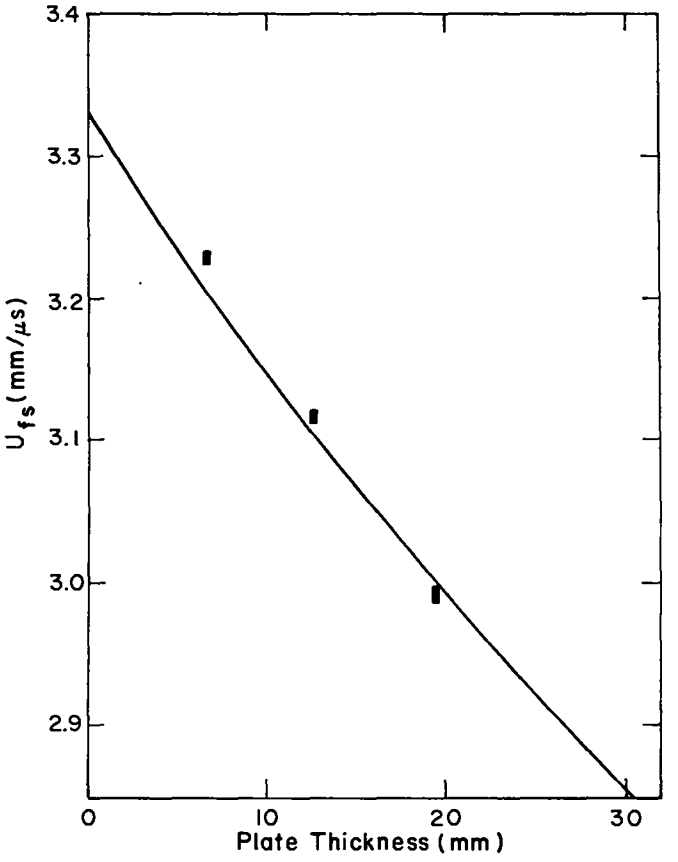

Fig. 5.2d. The free-surface velocity of 1100F Al plates induced by a 76-mm charge of Composition B.

Perfectly plastic 1100F Al
Hydrostat; LA-4167-MS
Our model ————
Warnes[34] data (average); ▮
Some of the experiments had Ta foils in the last 25 mm of explosive and in the 1100F Al. The presence of the foils does not appear to significantly effect the measured values.

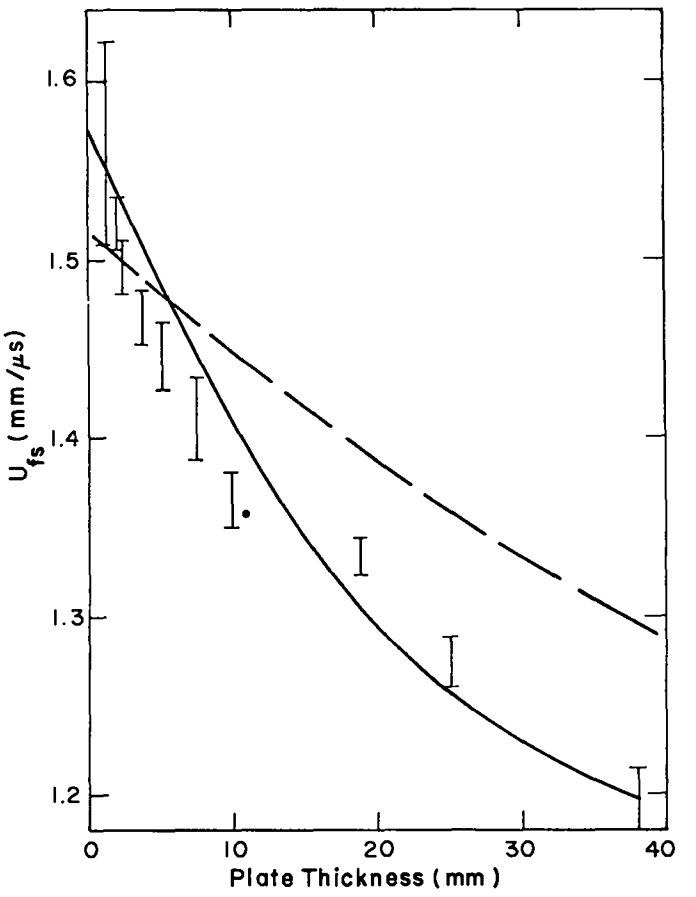

Fig. 5.3. The free-surface velocities induced into uranium by 203-mm of Composition B.

Elastic-plastic uranium
Hydrostat; Mie-Grüneisen ρ_o = 18.96 Mg/m^3, c_o = 2.487 mm/μs, s = 1.62, Γ = 2.2
Yield Strength;[35] 0.12 GPa
Shear Modulus;[35] 84.4 GPa
Chapman-Jouguet model —— ——
ρ_o = 1.73 Mg/m^3, D = 7.85 mm/μs, γ = 2.64

because they clearly show that side rarefactions are not an important consideration in these experiments. If, as has been argued, the steepness in the slope of $U_{fs}(x)$ for long (101 mm and 203 mm) charges was a result of the influence of side rarefactions on the flow, then the change in slope observed in the uranium data would not have been seen. The data on (60/40) brass also support our model. Figure 5.4 shows that our model is also consistent with these data, whereas the Chapman-Jouguet model is not.

The situation for magnesium is quite different. Although the calculation shown in Fig. 5.5 is in good agreement for plates less than 12-mm thick, the data and calculation are in considerable disagreement for thicker plates. The data suggest that the rarefaction in magnesium degrades the shock more slowly than is the case in our calculation. Considering the agreement obtained for the other inerts it seems unlikely that our calculation of the detonation wave in the explosive is incorrect. Also, since the time required to generate the reaction zone profile is reasonably long, it is not likely that

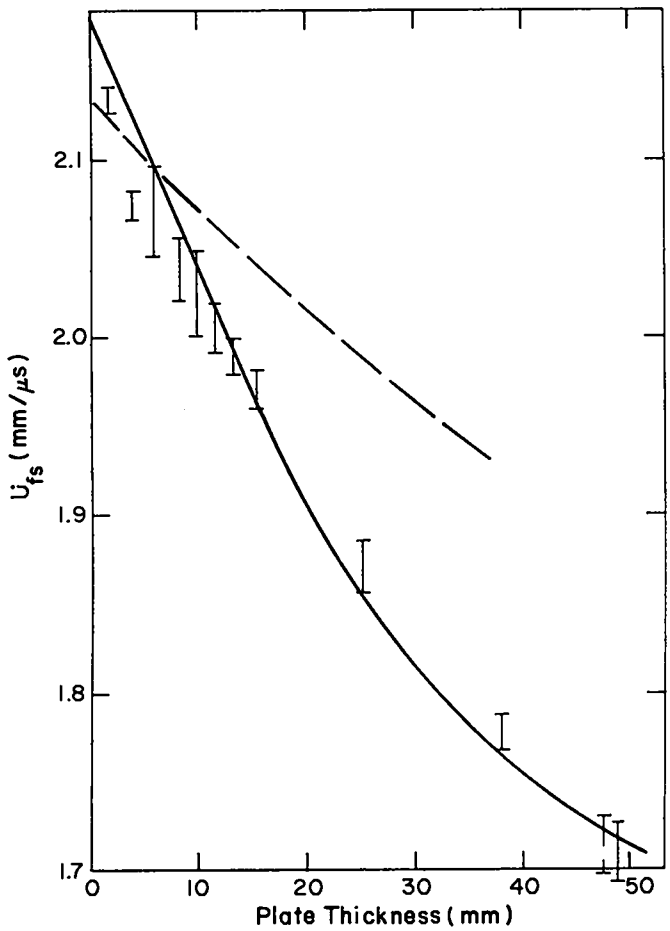

Fig. 5.4. The free-surface velocities induced into (60/40) brass by 203-mm of Composition B.

Brass Hydrostat; LA-4167-MS
Yield Strength;[36] 0.08 GPa
Shear Modulus;[36] 38.0 GPa
Chapman-Jouguet model ——— ———
ρ_o = 1.73 Mg/m^3, D = 7.85 mm/μs,
γ = 2.64

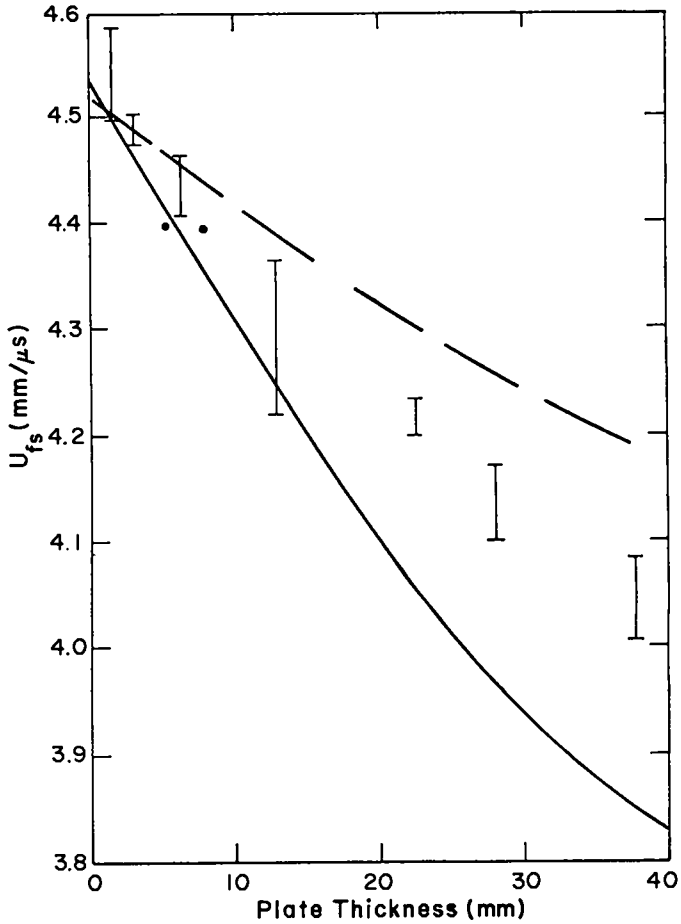

Fig. 5.5. The free-surface velocities induced into magnesium by 203-mm of Composition B.

Magnesium Hydrostat: LA-4167-MS
Yield Strength;[35] 0.17 GPa
Shear Modulus;[35] 16.5 GPa
Chapman-Jouguet model ——— ———
ρ_o = 1.73 Mg/m^3, D = 7.85 mm/μs,
γ = 2.64

forces acting at the interface (or their absence) could produce a significant change in the wave shape (speeding or quenching of the reaction by a shock or rarefaction). Nevertheless, it seems worthwhile to determine whether the impedance of the inert has any unexplained effect on $U_{fs}(x)$, since magnesium is almost a perfect match to the explosive whereas the other inerts reflect shocks into the explosive. One way of proceeding is to compare the results of calculation and experiment for an inert which reflects a rarefaction into the explosive as opposed to a shock. Figure 5.6 provides such a comparison using Plexiglas. Although the agreement leaves something to be desired, it is clear that the shape of the calculated curve and the data are in qualitative agreement. Considering that all of our calculations for the 203-mm long Composition B experiments are high compared to the experimental results, it would not be unreasonable to expect that a modified calibration (for example, an increase in γ) would yield better calculations not only for Plexiglas but for dural, brass, and uranium as well. All of this

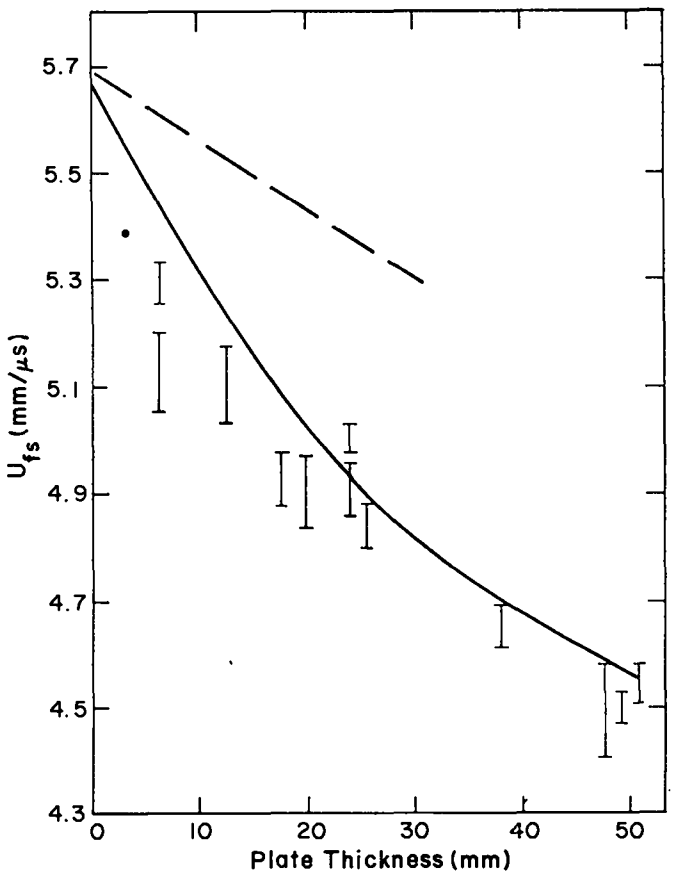

Fig. 5.6. The free-surface velocities induced into Plexiglas by 203-mm of Composition B.

Plexiglas Hydrostat; LA-4167-MS
Chapman-Jouguet model ——— ———
ρ_o = 1.73 Mg/m^3, D = 7.85 mm/μs,
γ = 2.64
The data was obtained by Deal using Plexiglas of density 1.179 Mg/m^3.

suggests that Plexiglas is consistent with our model and that the form of the incoming detonation wave is not sensitive to whether a shock or rarefaction is reflected into the explosive by the inert. Therefore, we are led to the conclusion that either our description of magnesium is not adequate or perhaps the data are in error.

Reviewing the results of these calculations we find that, with the exception of magnesium, our time-dependent model of Composition B is in agreement with the free-surface velocity measurements for a wide range of inerts and explosive lengths. This model is the simplest possible one which is consistent with both these measurements and the conservation laws. Since one expects that both the equations of state and the rate law(s) are in reality more complex than those used here, it is perhaps surprising that the agreement of calculation and experiment is as good as it is. In the next subsections we will show that this model is also consistent with a number of other (less sensitive) experiments that have been performed on Composition B.

C. The X-ray Experiments

The first set of experiments we will consider were those performed by Rivard et al.[19] in which the equation of state for Composition B products was determined. In these experiments a sandwich of 12.5 μm Ta foils and 6.35-mm pieces of Composition B was built up to a total height of 101 mm. Ten individual shots were fired with radiographs being taken of the initial foil positions and the foil positions at times corresponding to detonation runs ranging from 48 mm to 101 mm. Their analysis of these data demonstrated that no statistically significant differences could be resolved among the following possibilities: (1) a Chapman-Jouguet detonation, (2) a slightly time-dependent detonation, (3) a steady slightly weak detonation. Therefore, they assumed a Chapman-Jouguet detonation and showed that the following flow (Taylor wave) could be described by the two-parameter function

$$y_{rv} = 1 + a^{-1} \ln\left(\frac{aY+b}{a+b}\right) \tag{5.3a}$$

$$a = 0.634 \tag{5.3b}$$

$$b = 0.709 \ , \tag{5.3c}$$

where y and Y are the final and initial foil positions scaled with respect to the instantaneous location of the detonation front. Since the derivation of Eq. (5.3) requires no assumptions concerning an equation of state, they used it to check the ability of the standard calibrated equations of state at reproducing the radiographic data. Figure 5.7 shows $\Delta y \equiv y - y_{rv}$ vs Y for both our model and a number of the standard equation-of-state calibrations. This plot clearly shows that the standard calibration of the γ-law (P_{CJ} = 29.2 GPa) agrees with the data over the widest range while our model agrees only over a comparatively short range. Considering that the free-surface velocity measurements used to calibrate our model provide information on only the leading portion of the wave profile, some improvement

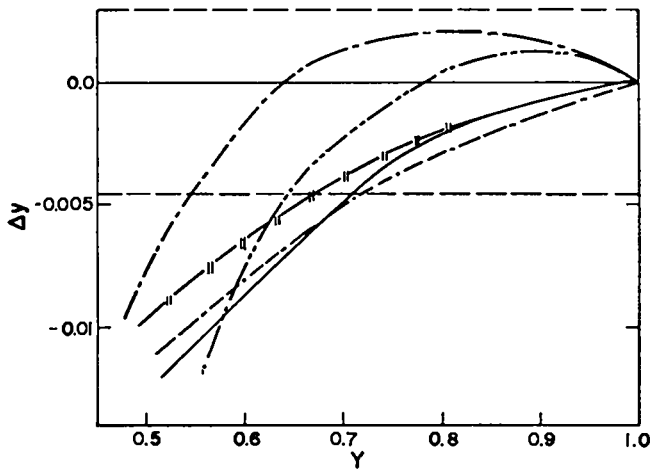

Fig. 5.7. A plot of Δy vs Y for two calibrated isentropes, our model, and a calibration of Eq. (5.3a) to some data obtained by Davis.[6]

JWL (P_{CJ} = 29.2 GPa)[19] ——— – – ———

γ-law (P_{CJ} = 29.2 GPa)[19] ——— – ———

The model with a constant γ = 3.15 rarefaction wave ———————

The model with a variable γ (3.15 - 2.45) rarefaction calculated using the JWLR[19] isentrope equivalent to Eqs. (5.3) as a reference ——— || ———

A calibration of Eq. (5.3a) to Davis' data (P_{CJ} = 26.8 GPa) ——— – – ——— – – ———

The heavy horizontal line is the reference (y_{rv}) and the two dashed horizontal lines bound the experimentally observed points

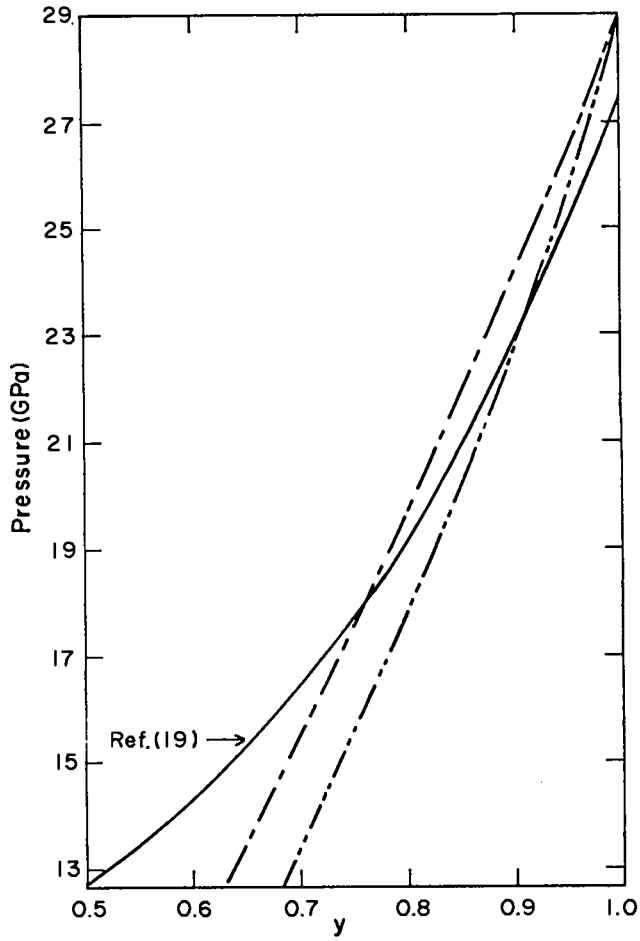

Fig. 5.8a. The pressure wave in Composition B vs the scaled distance (y).

Rivard (P_{CJ} = 27.5 GPa) ———————

γ-law (P_{CJ} = 29.2 GPa) ——— – – ———

JWL (P_{CJ} = 29.2 GPa) ——— – – ———

in our foil calculation could be achieved if the constant-γ rarefaction following our reaction zone were replaced by a calculation that uses a JWLR[19] isentrope equivalent to Eq. (5.3) as a reference. As is apparent from the figure, this calculation represents only a modest improvement over our previous one. Since this modest gain was obtained by decreasing γ in the rarefaction from 3.15 to 2.45, it does not seem likely that any reasonable equation of state will correct for the deficiency between our model and the data.

The better agreement obtained with the calibrated isentropes as compared to our model implies only that the average velocity of the foils calculated with these isentropes is about that observed experimentally. This is achieved not because of any real similarities between them but simply because the isentropes are calibrated to a Chapman-Jouguet pressure of 29.2 GPa while Rivard's value is 27.5 GPa. Considering that the free-surface velocity measurements give a front pressure of 28.2 GPa for a 101-mm charge of Composition B, the agreement achieved with the calibrated isentropes is probably suspect. A comparison of the pressure profiles after 12 μs of run reveals large differences between Rivard's profile and all of the others. Figure 5.8a shows that even though the pressure wave obtained with the calibrated isentropes and Rivard's fit are very different, the difference of 1.7 GPa in the Chapman-Jouguet pressure is sufficient to offset the difference and produce fair agreement in the foil

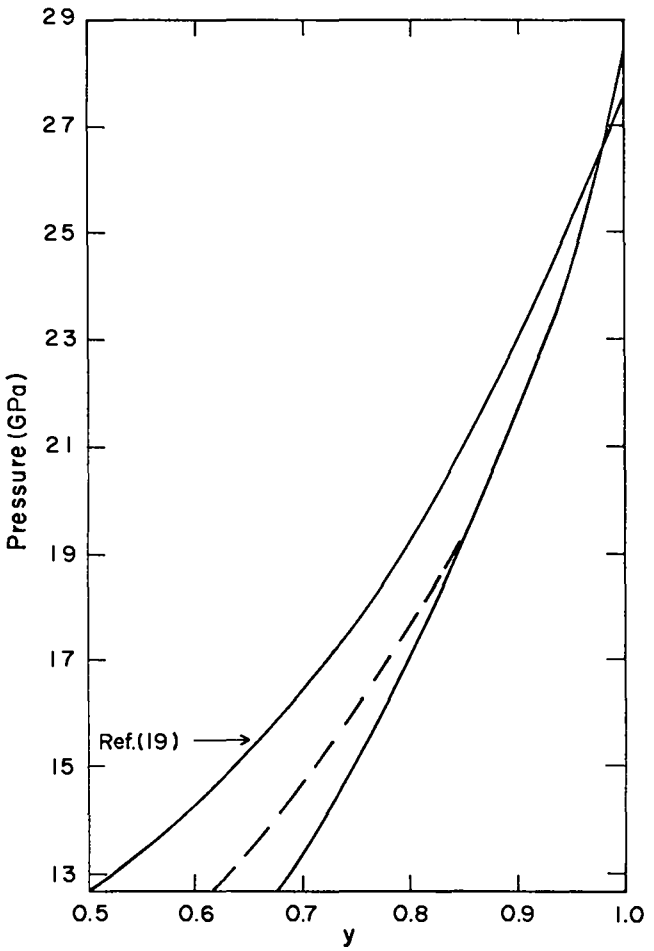

Fig. 5.8b. The pressure wave in Composition B vs the scaled distance after the detonation has run for 12 μs.

The model ([P] = 28.3 GPa) ———

The model with JWLR Taylor wave — —

positions. Similarly, Fig. 5.8b shows that although the agreement between our model and Rivard's flow is good close to the front, the steepness of our profile (being similar to that of the JWL) brings about the rather poor agreement at the low-pressure end.

The comparatively shallow gradient in their fit pressure wave is a result of the rapid decrease of $\gamma = -\left(\frac{\partial \ln P}{\partial \ln v}\right)_S$ from 2.96 $\left[\rho_o\left(\frac{d\gamma}{d\rho}\right)_S = 0.8\right]$ at the front to 1.69 $\left[\rho_o\left(\frac{d\gamma}{d\rho}\right)_S = 7.1\right]$ at 13 GPa. Even though no physical constraints are violated in their fit, the rapid change in γ which it predicts is intuitively very unappealing. Considering that nearly 2% of the total mass of the explosive charges used in these experiments consists of layers of Ta foils, one has no assurance that the results obtained by Rivard et al. are not influenced by this nontrival perturbation.

Another relatively new x-ray technique[37] provides us with an independent check of the applicability of Rivard's flow field. This method is especially attractive because foils are not used. Instead a series of three parallel small rectangular parallelepipeds 1.5-mm square by 101-mm long and 10-mm apart are machined into the explosive with their major axis aligned parallel to the detonation front. The rarefactions generated when the detonation wave encounters these voids are of sufficient strength so that their location at any time can be resolved on a radiograph. In themselves these radiographs are of little value because the location of the two-dimensional wave fronts generated by the voids is a complicated function of the time-dependent flow field which the waves experience. Assuming that the signals generated by the voids obey the laws of geometrical acoustics, Engelke[38] has shown that the wave patterns can be calculated once the flow field is known. Of particular interest to us is the comparison of some calculations of Engelke[39] on Composition B with the experimental radiographs. Figure 5.9 shows the calculation using the flow of Eq. (5.3) and the experimental data. The calculation produces wave fronts which are different from the data. Most striking is the lag of the backward-going ray for the largest acoustic ring. Although the location of the wave is a complicated function of the gradients of the flow variables as well as the variables themselves, the observed lag is in large measure due to the rapidly decreasing value of the sound speed in Rivard's flow. Considering that the theoretical analysis is probably an adequate description of reality and that the perturbations that have been introduced are considerably less than those introduced by the foils, there is some reason to question the results of the foil experiments. Replacing the flow field by the $O(\delta)$ approximation to our time-dependent detonation model, we find that the agreement between calculation and experiment is good (see Fig. 5.10). Therefore, these experiments support our

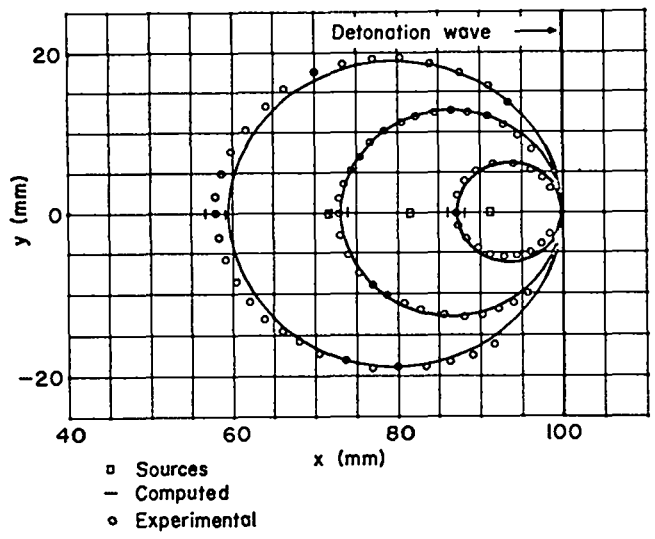

Fig. 5.9. A calculation of the wavefronts in a 101-mm-long charge of Composition B using Eqs. (5.3) for the flow field. The error bars represent the thickness of the rarefaction wave observed on the radiograph.

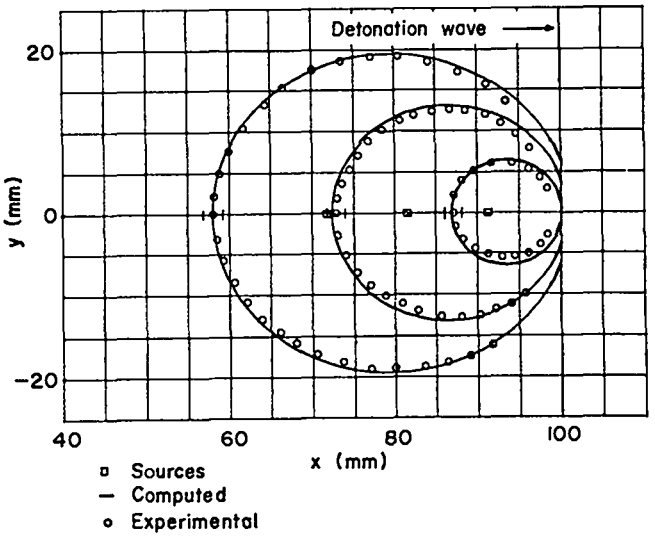

Fig. 5.10. A calculation of the wavefronts in a 101-mm-long charge of Composition B using the $O(\delta)$ approximation to our time-dependent detonation model with $D^* = 7.85$ mm/μs, $\gamma = 3.15$, $\delta = 0.16$, $k_2 = 2\ \mu s^{-1}$. The flow in the Taylor wave uses a constant γ equation of state.

model and imply that the flow determined by the foil experiments may not properly describe Composition B.

A third set of x-ray experiments also supports our model. Using a 101-mm-long charge abutted against a Plexiglas plate, Davis and Venable[6] measured the location with time of the plane backward-facing rarefaction generated at the material interface. This experiment has certain advantages as well as disadvantages. Its primary advantage is that it does not introduce any perturbations on the original detonation wave as the other x-ray techniques do. The chief disadvantage is that the wave velocity being measured (c-u) does not yield very much information about the flow. The average value of (c-u) obtained in the experiment as well as those calculated with our model and Eq. (5.3)

$$(c-u)_{exp} = 4.00 \pm 0.08 \text{ mm/μs} \qquad (5.4a)$$

$$(c-u)_{Eq.\ (5.3)} = 3.80 \text{ mm/μs} \qquad (5.4b)$$

$$(c-u)_{model} = 4.02 \text{ mm/μs} \qquad (5.4c)$$

provide additional support for our model. Again we find that the result obtained from the foil experiment is significantly different from the experimental value. The deficiency of 0.2 mm/μs from the experimental value is in agreement with the results of the calculation displayed in Fig. 5.9. This serves to further corroborate our argument that the flow field obtained from the analysis of the foil experiments may in some way be perturbed by the foils.

Summarizing, we find that these experiments show that the wave profiles obtained with the foil experiments do not agree with those obtained with the other x-ray techniques. The region of reactive flow which our model postulates is in agreement with all of the direct measurements of the flow that have been made using all three x-ray techniques, and a $\gamma = 3.15$

TABLE V-1

SHOCK TRANSIT TIMES IN DURAL[a]

x/2X	X = 25 mm t (μs)/2	X = 51 mm t (μs)/4	X = 102 mm t(μs)/8
0.025	0.085 ± 0.005[b]	0.085[b]	0.084
		0.088[c]	0.085
		0.085[d]	0.085
0.050	0.171	0.170	0.169
		0.172	0.171
		0.168	0.169
0.075	0.259	0.256	0.254
		0.257	0.254
		0.254	0.253
0.100	0.347	0.344	0.341
		0.343	0.340
		0.341	0.339
0.125	0.439	0.432	0.427
		0.429	0.427
		0.427	0.424

[a]Transit times for Composition B induced shocks in dural. X is the length of explosive and x the thickness of the plate. The diameter of the explosive is 101 mm. The deviation is our estimate of the errors. All calculations were done with elastic-plastic dural (see Sec. IV.C).

[b]Finger and Kurrle[17]

[c]Our model

[d]Chapman-Jouguet model
X = 51 mm P_{CJ} = 26.8 GPa (ρ_o = 1.73 Mg/m^3, D = 7.85 mm/μs, γ = 2.98)
X = 102 mm P_{CJ} = 28.4 GPa (ρ_o = 1.73 Mg/m^3, D = 7.85 mm/μs, γ = 2.76)

rarefaction wave is consistent with all but the foil experiments. Therefore, we conclude that our model is also consistent with all of the x-ray data on Composition B.

D. Shock Transit Times

The last set of experiments on Composition B that we consider are the shock transit time data obtained by Finger and Kurrle.[17] Using the electrical probe technique devised by Hayes,[16] they measured the transit time of a Composition B induced shock in both dural and PMMA. Their results are compared to values obtained with our model and the Chapman-Jouguet model in Tables V-1 and V-2. For the case of dural the values are indistinguishable. The situation for Plexiglas is not as good. A comparison of the experimental data and calculation reveals that the experimental shock velocity is considerably higher than the calculated values. Kurrle's measured value of the shock velocity in PMMA is 6.955 mm/μs. If we assume the equation of state for

TABLE V-2

SHOCK TRANSIT TIMES IN PLEXIGLAS[a]

x/2X	X = 25 mm t (μs)/2	X = 51 mm t (μs)/4	X = 102 mm t (μs)/8
0.025	0.089 ± 0.005[b]	0.091[b]	0.092
		0.090[c]	0.092
0.050	0.186	0.186	0.188
		0.191	0.193
0.075	0.285	0.285	0.286
		0.289	0.294
0.100	0.384	0.384	0.385
		0.394	0.396
0.125	0.484	0.483	0.489
		0.497	0.503

[a]Transit times for Composition B induced shocks in Plexiglas. The diameter of the explosive is 101 mm. The calculations used Plexiglas (LA-4167-MS). The experiments were done with 76.2-mm-diameter cast acrylic plastic bar (clear), product code 2101, Cadillac Plastic Co. The product specification sheet gives a specific gravity range of 1.17 - 1.20. Its equation of state is unknown.

[b]Finger and Kurrle[17]

[c]Our model

Plexiglas given in (LA-4167-MS) then $u_s(0) \geq 2.88$ mm/μs which in turn implies that $U_{fs|o} \geq 5.95$ mm/μs. Comparing this with Deal's measured value for a 203-mm-long charge of Composition B, we find it to be incompatible with his result ($U_{fs|o} \leq 5.66$ mm/μs). Part of the problem may stem from the fact that Kurrle used a commercial grade cast acrylic bar and not Plexiglas Type II (see the caption accompanying Table V-2). Considering the large discrepancies between the measured and computed shock velocity and the lack of a precise specification of their inert, a valid comparison of the model with this experiment cannot be made for PMMA.

E. Overview

The results that we have just presented demonstrate that our model successfully describes a variety of different types of experiments that have been performed on Composition B. Particularly significant is its ability to reproduce the free-surface velocities of dural plates driven by both short (25 mm) and long (203 mm) charges of explosive. In addition, it also reproduces the free-surface velocities induced by long charges into other inerts ranging from uranium to Plexiglas. The modifications of the simple theory which lead to these improvements were shown to also be consistent with the results of some

of the more insensitive experiments (x-ray techniques, shock transit times).

All of this was the result of our assumption that the detonation is driven by a very fast and exothermic reaction which is then followed by a relatively slow, weakly energetic (exothermic) one. This leads to the following picture of detonating Composition B. Because it is slow, at early times (short charges) the second reaction contributes little to the process and consequently the flow at the end of the first reaction zone (which is taken to be infinitesimally thin) is sonic with the pressure there being 25.6 GPa. With the passing of time the heat liberated by the second reaction begins to make a positive contribution to the detonation. The sonic plane falls behind the end of the first reaction zone and the pressure at the end of the first reaction increases. In the limit of long times the reactive flow reaches a steady state. The sonic plane is then located at the end of the second reaction, where the pressure (the Chapman-Jouguet pressure) is equal to 26.3 GPa while at the end of the first reaction it is up to 30.4 GPa. Therefore, the Chapman-Jouguet pressure of Composition B (as determined by our model) is approximately 26 GPa. Also, since the detonation velocity depends on the amount of energy released ahead of the sonic plane, our model predicts that it will increase 100 m/s in going from short to the very longest charges (70 m/s in going from 12.7 mm to 203 mm).

The Chapman-Jouguet pressure of Composition B determined from our model is the lowest value that has yet been reported. Perhaps it is fortuitous, but this value is in excellent agreement with the value Fickett[40] obtained with his LJD calculation of the equation of state of Composition B detonation products

Fickett: $\rho_o = 1.714$ Mg/m^3 (65%/35%) (5.5a)

$P_{CJ} = 25.9$ GPa (5.5b)

$U = 7.987$ mm/μs (5.5c)

$\gamma = 3.22$ (5.5d)

Model: $\rho_o = 1.73$ Mg/m^3 (60%/40%) (5.6a)

$P_{CJ} = 26.3$ GPa (5.6b)

$U = 7.95$ mm/μs (5.6c)

$\gamma = 3.15$. (5.6d)

Since Fickett's theory is based on first principles (equation of state derived from forces of intermolecular interaction) the agreement of our model with his theory is an encouraging result. Perhaps even more interesting are the results of some experiments that were recently performed by Davis.[41] Using an optical technique he was able to measure the detonation velocity to within ± 20 m/s in a planewave Composition B assembly. He found that, as predicted, the detonation velocity increased (86 m/s) in going from a 12.7-mm charge (7.869 mm/μs) to a 203-mm charge (7.955 mm/μs). Considering that the free-surface velocity data used in the calibration of our model was somewhat noisy and that the calibration is not sensitive to small changes in D^* and γ, the calculated values of 7.85 mm/μs and 7.92 mm/μs are in excellent agreement with experiment.

These results are all very encouraging. They imply that not only are we able to model the results of a few experiments, but more importantly that real progress has been made at understanding the basic underlying physical processes. Such an understanding is particularly important if one is interested in performing calculations on explosives in geometries that are very different from those on which calibrations are made. We have not attempted to define precisely the nature of the second rate process in our model. However, now that a few properties of the process are known, progress in this direction becomes a more realistic possibility.

VI. CALIBRATION OF OUR MODEL TO PBX-9404

The plastic-bonded solid explosive PBX-9404-03 also exhibits nonideal behavior. Craig[5] showed that the free-surface velocity curves which result when PBX-9404 interacts with either dural or Plexiglas show both an increasing $U_{fs}|_o$ with run and an anomalous slope (too steep) for long runs. Since our time-dependent model successfully accounts for similar behavior in Composition B, we recalibrated it to Craig's PBX-9404 data. We obtain

$D^* = 8.60$ mm/μs (6.1a)

$k_2 = 2.0$ μs^{-1} (6.1b)

$\gamma = 3.30$ (6.1c)

$\delta = 0.258$. (6.1d)

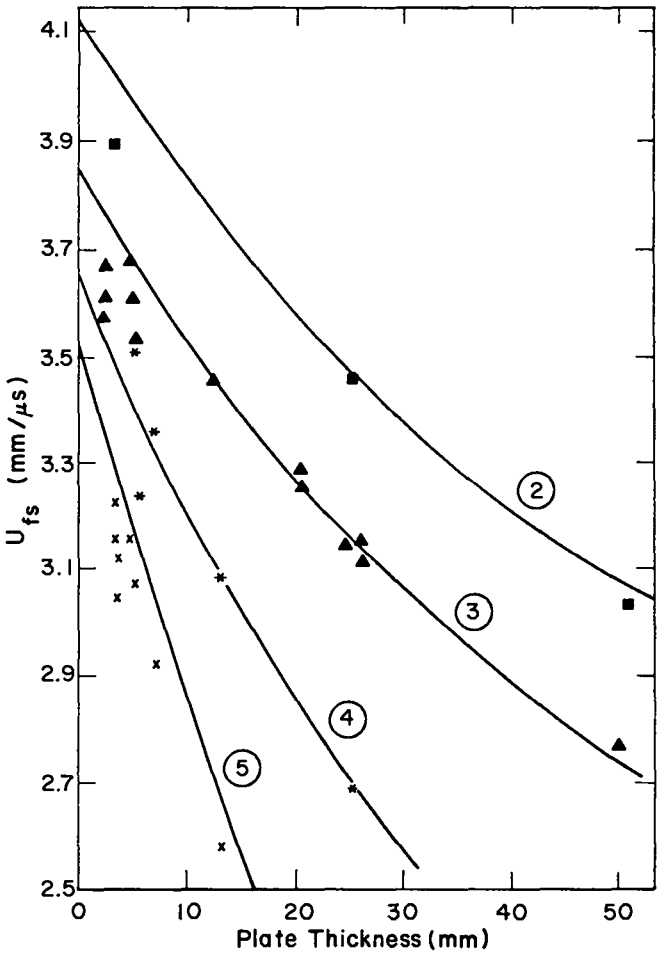

Fig. 6.1. The PBX-9404/dural free-surface velocities. Calculated curves 2,3,4,5 correspond to explosive lengths of 101 mm, 50.8 mm, 25.4 mm, and 12.7 mm respectively. Equations (6.1) describe the explosive and the dural is

Hydrostat; LA-4167-MS
Yield Strength; 0.3 GPa
Shear Modulus; 25 GPa
Craig's[5] data
■ - 101 mm long PBX-9404
▲ - 50.8 mm
✱ - 25.4 mm
X - 12.7 mm

Comparing these constants to Eqs. (5.2) we find that the most significant change is the increase of 0.1 in δ. This corresponds to an increase in the energy of the second reaction from 2.5% in Composition B to 6.2% in PBX-9404. In turn this results in a second reaction zone which is more subsonic at late times, and a larger increase in the detonation velocity with run (12.7 mm - 8.61 mm/μs, 101 mm - 8.74 mm/μs, ∞ - 8.87 mm/μs).

Figures 6.1 and 6.2 compare the results of calculation and experiment. The overall agreement is good for both dural and Plexiglas. As for Composition B, the shock transit times computed with our model agree with the experimental values of Finger and Kurrle[17] (see Tables VI-1 and VI-2). Because of the excellent agreement between these calculations

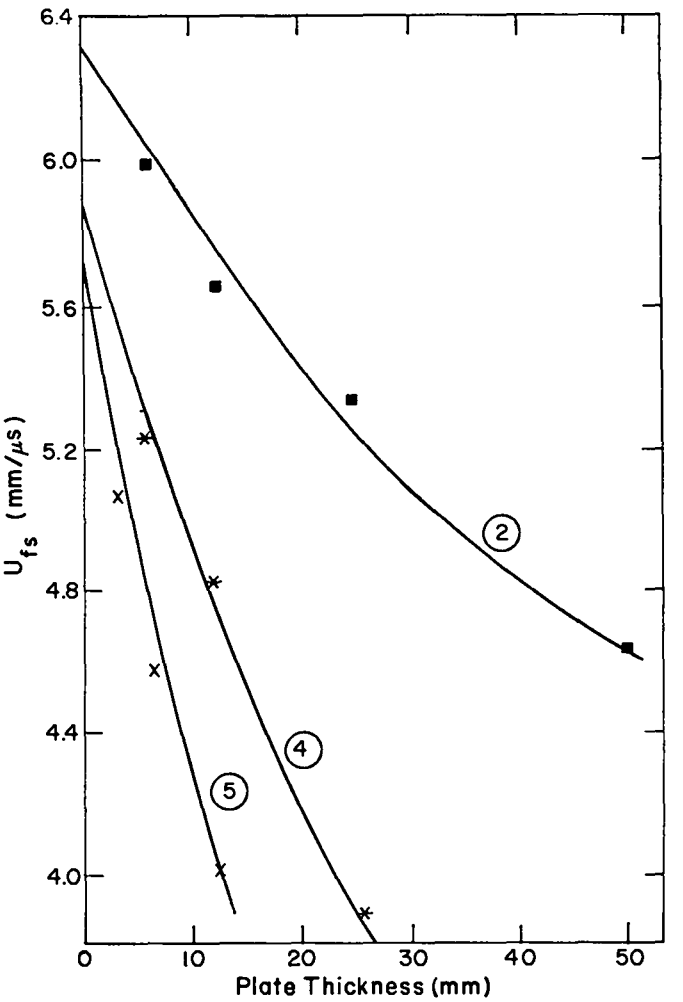

Fig. 6.2. The PBX-9404/Plexiglas free-surface velocities. Calculated curves 2,4,5 correspond to explosive lengths of 101 mm, 25.4 mm, and 12.7 mm respectively. Equations (6.1) describe the explosive. The Plexiglas hydrostat is found in LA-4167-MS.

Craig's[5] data
■ - 101 mm long PBX-9404
✱ - 25.4 mm
X - 12.7 mm

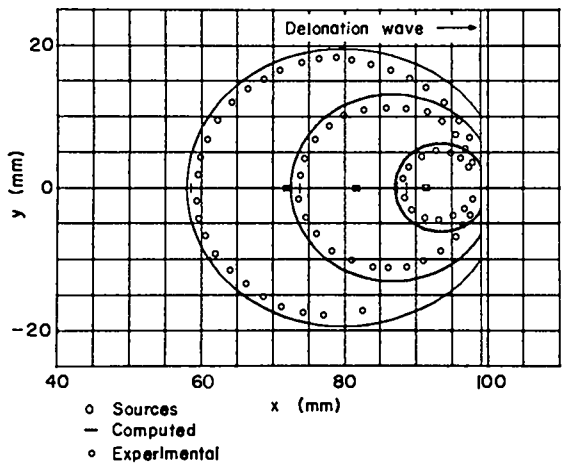

Fig. 6.3. A calculation of the wavefronts in a 101-mm long charge of PBX-9404 using the $0(\delta)$ approximation to our time-dependent detonation model with $D^* = 8.60$ mm/μs, $\gamma = 3.30$, $\delta = 0.258$, $k_2 = 2\ \mu s^{-1}$. The flow in the Taylor wave uses a constant γ equation of state.

and experiment one might be tempted to conclude that our model also provides an accurate description of PBX-9404. The following results show that our expectations have exceeded our grasp. Calculations made with our $0(\delta)$ model for PBX-9404 are in striking disagreement with the experimental radiographs (see Fig. 6.3). The experimental data show no ring opening (indicating that we have a sonic plane very near the front), whereas the calculations show a substantial opening. Also, recent measurements of the detonation velocity in PBX-9404[41] show that it does not increase with run, as predicted, but is constant at 8.735 ± 0.02 mm/μs. Therefore, although our model reproduces the free-surface velocity and shock transit times for PBX-9404, its reaction zone structure is not consistent with all of the existing data.

TABLE VI-1

SHOCK TRANSIT TIMES IN DURAL[a]

x/2X	X = 12.7 mm t (μs)	X = 25 mm t (μs)/2	X = 51 mm t (μs)/4	X = 102 mm t (μs)/8
0.025	0.077 ± 0.007[b]	0.077[b]	0.079	0.078
	0.081	0.079[c]	0.080	0.082
0.050	0.159	0.166	0.161	0.162
	0.160	0.159	0.161	0.161
0.075	0.241	0.249	0.245	0.244
	0.242	0.242	0.242	0.242
0.100	0.325	0.339	0.329	0.328
	0.323	0.324	0.324	0.323
0.125	0.410	0.426	0.415	0.412
	0.407	0.408	0.407	0.405

[a] Transit times for PBX-9404 induced shocks in dural. X is the length of explosive and x the thickness of the plate. The diameter of the explosive is 101 mm.

[b] Finger and Kurrle[17]

[c] Our model

TABLE VI-2

SHOCK TRANSIT TIMES IN PLEXIGLAS[a]

x/2X	X = 12.7 mm t (μs)	X = 25 mm t (μs)/2	X = 51 mm t (μs)/4	X = 102 mm t (μs)/8
0.025	0.085	0.088[b]	0.089	0.089
	0.087	0.086[c]		0.090
0.050	0.179[c]	0.180[c]		0.179[c]
0.075	0.274	0.277		0.273
0.100	0.371	0.372		0.366
0.125	0.469	0.470		0.464

[a] Transit times for PBX-9404 induced shocks in Plexiglas. X is the length of explosive and x the thickness of the plate. The diameter of the explosive is 101 mm.

[b] Finger and Kurrle[17]

[c] Our model

This negative result is of considerable value. First, it serves to warn the model user that any model which does not provide an accurate picture of the physics of the detonation must be considered nothing more than an empirical fit to a restricted set of data. As such, its use should be limited to interpolation. Second, our model's inability to produce simultaneously a pressure buildup with run and a constant detonation velocity suggests certain modifications. The constancy of the detonation velocity implies that the flow must be sonic at the end of the first reaction zone. The observed buildup suggests that some relatively slow exothermic process must occur behind this sonic plane. A model capable of yielding the desired behavior was discussed in Sec. III.A. This is achieved by following the first chemical reaction by two parallel reactions that satisfy the condition

$$q_2 r_2 + q_3 r_3 = 0 \qquad (6.2)$$

at the end of the first reaction and

$$q_2 + q_3 > 0 \quad . \tag{6.3}$$

The two-wave structure that is produced by this reaction scheme is currently being studied.

VII. SUMMARY

It has been known for some time that the free-surface velocity data on planewave Composition B do not scale. Experiments show that the intercepts $U_{fs}|_o$ increase with the length of the charge and that the slopes $\frac{dU_{fs}}{dx}$ for long charges are too steep compared to those obtained with the Chapman-Jouguet theory. Our review of these data showed that side rarefactions must be ruled out as the cause for the observed discrepancies between the data and calculation and that the observed differences are a result of the failure of the Chapman-Jouguet theory. By assuming that Composition B obeys the following one-dimensional time-dependent model we were able to bring the calculated and experimental $U_{fs}(x)$ curves into agreement.

(1) The detonation in Composition B is controlled by two rate processes.

(2) The first process is irreversible, very fast (instantaneous) and releases 97.5% of the available energy.

(3) The second step is slow ($k_2 = 2.0\ \mu s^{-1}$) and yields the remaining 2.5% of the energy.

(4) The region of reactive flow is followed by a γ-law ($\gamma = 3.15$) Taylor wave.

In addition to reproducing the $U_{fs}(x)$ data, this model was also shown to be consistent with all of the other data on this explosive. Implicit in the assumptions of our model is that the detonation velocity increases with run (70 m/s in going from 12.7 mm to 203 mm of explosive). Recent experiments confirm this prediction. In light of all these results we conclude that our time-dependent model provides a reasonable physical description of Composition B. Using this model to interpret the $U_{fs}(x)$ data we find that the Chapman-Jouguet pressure for Composition B is $P_{CJ} = 26.3$ GPa ($\rho_o = 1.73\ Mg/m^3$, $U = 7.95$ mm/μs).

This model was also calibrated to PBX-9404. By releasing 6.2% of the total energy in the slow kinetic step we were able to reproduce all of the free-surface velocity data for this explosive. However, since the predicted increase in the detonation velocity was not observed experimentally, this model was judged to be unacceptable for PBX-9404. There are indications that this model will be useful for TATB and nitroguanidine. Radiographs of these explosives show that the flow behind the detonation front is quite subsonic. This in turn suggests the presence of a long second reaction zone similar to that used in our model. Unfortunately the limited data which are available for these explosives do not permit us to test our theory.

This study probably raises more questions than it answers. One is presented with the problem of identifying the nature of the second rate process in Composition B. Calculations on both the probable rate of carbon coagulation and turbulence dissipation should be carried out to determine if either of these processes are likely candidates. Of even more interest is the result that the slow processes which are responsible for the detonation wave structure in Composition B and PBX-9404 are apparently quite different. Calculations are currently under way to determine if the two-wave structure alluded to in Sec. VI might not account for the observed behavior in PBX-9404.

ACKNOWLEDGEMENTS

The authors would like to thank B. G. Craig, R. P. Engelke, W. Fickett, J. D. Jacobson, and C. L. Mader for their valuable suggestions concerning this work.

REFERENCES

1. D. R. White, Phys. Fluids 4, 465 (1961).

2. W. C. Davis, B. G, Craig, and J. B. Ramsay, Phys. Fluids 8, 2169 (1965).

3. W. W. Wood and W. Fickett, Phys. Fluids 6, 648 (1963).

4. R. W. Goranson, Los Alamos Scientific Laboratory, internal report, 1945.

5. B. G. Craig, Los Alamos Scientific Laboratory, unpublished data, 1965.

6. W. C. Davis and Douglas Venable, "Pressure Measurements for Composition B-3," Fifth Symposium on Detonation, 1970. ACR-184. U. S. Gov't Printing Office.

7. W. C. Davis and W. C. Rivard, Los Alamos Scientific Laboratory, unpublished data, 1970.

8. W. E. Deal, J. Chem. Phys. 27, 796 (1957).

9. C. L. Mader and B. G. Craig, Los Alamos Report, LA-5865 (1975).

10. C. L. Mader, Los Alamos Scientific Laboratory, internal report, 1968.

11. R. E. Duff and E. Houston, J. Chem. Phys. 23, 1268 (1955).

12. W. E. Deal, Phys. Fluids 1, 523 (1958).

13. W. E. Deal, Private Communication.

14. W. C. Davis, Los Alamos Scientific Laboratory, unpublished data, 1970.

15. R. H. Warnes, Los Alamos Scientific Laboratory, unpublished data.

16. B. Hayes, J. Appl. Phys. 38, 507 (1967).

17. M. Finger and J. Kurrle, Private Communication, J. E. Kurrle, et al., Progress Report for Lawrence Radiation Laboratory, SANL No. 813-002 (1970).

18. D. Venable and T. J. Boyd, Jr., Fourth Symposium on Detonation, 1965. ACR-126. U. S. Gov't Printing Office.

19. W. C. Rivard, D. Venable, W. Fickett, and W. C. Davis, "Flash X-ray Observation of Marked Mass Points in Explosive Products," Fifth Symposium on Detonation, 1970. ACR-184. U. S. Gov't Printing Office.

20. B. Hayes and J. N. Fritz, "Measurement of Mass Motion in Detonation Products by an Axially-Symmetric Electromagnetic Technique," Fifth Symposium on Detonation, 1970. ACR-184. US Gov't Printing Office.

21. W. C. Davis and A. Vigil, Los Alamos Scientific Laboratory, unpublished data.

22. W. C. Davis, Los Alamos Scientific Laboratory, unpublished data.

23. M. L. Wilkins, Lawrence Livermore Laboratory Report UCRL-7322 (1963).

24. C. Truesdell and R. A. Toupin, The Encyclopedia of Physics, Vol. III/1, p. 491, S. Flügge, Ed. Springer Verlag, Berlin (1960).

25. R. M. Bowen, Arch. Rat. Mech. Anal. 33, 169 (1969).

26. J. J. Erpenbeck, "Theory of Detonation Stability," Twelfth Symposium on Combustion, The Combustion Institute, Pittsburgh, July 1968.

27. J. Bdzil and W. C. Davis, Los Alamos Scientific Laboratory, unpublished data.

28. W. W. Wood and F. R. Parker, Phys. Fluids 1, 230 (1958).

29. Wildon Fickett and Jack D. Jacobson, PAD3 1-D Hydro Code, Private Communication.

30. Wildon Fickett and Jack Jacobson, Private Communication.

31. R. Kinslow, Ed., High Velocity Impact Phenomena, Academic Press, New York, 1970, p. 530-68.

32. William Prager and P. G. Hodge, Theory of Perfectly Plastic Solids, Wiley, New York, 1951.

33. R. Moore and R. K. Zeigler "PACKAGE," Los Alamos Report LA-2367 (1959).

34. R. C. Warnes, Los Alamos Scientific Laboratory, unpublished data.

35. David J. Steinberg and Michael W. Guinan, "Constitutive Relations for the Kospall Code," Lawrence Livermore Laboratory Report, UCID-16226 (1973).

36. Estimates.

37. W. C. Davis, Los Alamos Scientific Laboratory, unpublished data.

38. R. P. Engelke, Los Alamos Scientific Laboratory, unpublished data.

39. J. B. Bdzil and Ray Engelke, Los Alamos Scientific Laboratory, unpublished data.

40. Wildon Fickett, Los Alamos Report, LA-2712, (1962).

41. W. C. Davis, Los Alamos Scientific Laboratory, unpublished data.

☆ US GOVERNMENT PRINTING OFFICE: 1975—677-182/60